From Department of Neuroscience
Karolinska Institutet, Stockholm, Sweden &
Ming Wai Lau Centre for Reparative Medicine, Karolinska Institutet, Hong Kong

NOVEL FLUORESCENT TOOLS AND TECHNIQUES FOR 3D IMAGING OF THE CLEARED BRAIN

Alex Yu Hin Wong

Karolinska Institutet

Stockholm 2023

Published by Karolinska Institutet.
Printed by Universitetsservice US-AB, 2023

ISBN **978-91-8016-927-1**
Cover illustration: Edited photograph of Hito Bielschowsky OptimStain™ silver stain (left) and silver-AIE stain (right) of mouse brain paraffin sections.

Novel Fluorescent tools and techniques for 3D imaging of the cleared brain

Thesis for Doctoral Degree (Ph.D.)

By

Alex Yu Hin Wong

The thesis will be defended in public at Inghesalen, floor 2 in Widerströmska huset on Friday, March 17th, 2023, at 9:30 am.

Principal Supervisor:
Assistant Professor Sijie Chen
Karolinska Institutet
Ming Wai Lau Centre for
Reparative Medicine

Co-supervisor(s):
Professor Ola Hermanson
Karolinska Institutet
Department of Neuroscience

Professor Per Uhlén
Karolinska Institutet
Division of Molecular Neurobiology

Opponent:
Dr. Iben Lundgaard
Lund University
Department of Experimental Medical Science

Examination Board:
Dr. Anna-Lena Ström
Stockholm Universitet
Department of Biochemistry and Biophysics

Dr. Anna Herland
KTH Royal Insitute of Technology in Stockholm
Department of Micro and Nanosystem at the
Royal Institute of Technology

Dr. Hans Blom
KTH Royal Insitute of Technology in Stockholm
Department of Applied Physics

To my friends and family

Popular science summary of the thesis

The brain is probably the most complex system in the universe. When something goes wrong with a system, we need a blueprint or map to navigate the problem and fix it. Building comprehensive maps of the brain would help us to recognize different cells and their locations so we can better understand how they connect and work with each other. Visualizing the human brain at high resolution in three-dimensions (3D) would help us to study how the brain functions and malfunctions across a broad range of neurological diseases. We could evaluate the shape, connections, and spatial organization of neurons with other cell types and fine structures in the brain.

Generating these 3D maps within a reasonable timescale could be achieved with fluorescence imaging whilst keeping the brain intact and transparent through "clearing methods". Tissue can become optically transparent by reducing the scattering of light using solvents or by removal of lipids etc. Fluorescent labelling techniques and optical sectioning microscopy can image intact tissue at the mesoscale in a reasonable amount of time. Although electron microscopy has its own key advantages, it only takes a light-sheet fluorescent microscope minutes to hours to image the whole mouse brain opposed to many months for a cubic millimeter with an electron microscope. Aggregation-induced emission (AIE) based dyes which are bright and photostable are suitable probes to be added to the fluorescent toolbox for 3D imaging of neurons and myelinated fibers in rodents.

This thesis aims to develop novel staining and imaging methods using AIE fluorescent chemical probes for 3D neuroimaging. These staining and imaging methods based on AIE probes can provide good contrast and photostability while also being compatible with tissue-clearing methods. We envision the future application of these methods in studying the archived brain tissues where genetic, toxin and viral tracers are not applicable.

Paper I: The development and optimization of a new silver technique using the fluorescent silver-ion sensitive **TPE-4TA** probe for fluorescent visualization of silver-stained proteins separated by SDS-PAGE which was evaluated against SYPRO Ruby and a traditional chromogenic silver nitrate stain.

Paper II: Following up on the technique from paper I the fluorescent silver method was adapted as a histological stain for neurons and fibers for visualization of the fixed mouse brain in paraffin tissue sections and 3D cleared tissue.

Paper III: This study demonstrated a new AIE-based fluorescent tool with near-infrared emission for selective imaging of myelinated fibers in cryosections, cleared mouse brain and teased sciatic nerves.

Abstract

Background: To better understand the complexity of the brain and how it becomes impaired under different pathological states, a considerably large number of brains would be needed for imaging to generate highly detailed maps in 3D. Chemical probes can offer a readily scalable labelling method that is robust, easy to use with the quick operation, and feasible for human tissue where genetic viral and toxin tracers are inappropriate. The drawbacks of immunostaining methods have spurred interest in developing alternative strategies to visualize the optically transparent brain, especially from fixed archived samples or human autopsies that are not optimally fixed.

Purpose: We envision AIE-based probes and techniques as robust tools when paired with clearing methods for visualizing the human brain. This thesis aims to develop alternative strategies to tissue labelling using novel AIE-based fluorescent chemical probes and methods that offer easy operation, high brightness, photostability and contrast suitable for 3D visualization of neurons and nerve fibers in mouse brains.

Paper I: The novel water-soluble silver-ion sensitive AIE probe TPE-4TA achieved by tetrazole-Ag^+ coordination, allowed for the development of a new fluorescent silver (silver-AIE) method to visualize separated proteins following sodium dodecyl-sulphate polyacrylamide gel electrophoresis (SDS-PAGE). Compared with conventional silver nitrate stains, silver-AIE not only offers sensitive fluorogenic detection of proteins, but it is quantifiable, easy to use, has a broad linear dynamic range and a great contrast which rivals the popular commercial stain, SYPRO Ruby. Study II describes how to troubleshoot the fluorescent silver gel stain, alternative steps for rapid staining and techniques to carry out the procedure correctly to avoid suboptimal results.

Paper II: We report a novel fluorescent silver stain for fixed mouse brain tissue compatible with multiplexed immunofluorescence imaging in paraffin sections. The Ag^+-specific aggregation-induced emission (AIE) strategy outperforms the chromogenic detection employed by many conventional silver staining protocols to visualize neurites and fiber tracts in paraffin sections or passive Clear Lipid-exchanged Acrylamide-hybridized Rigid Imaging / Immunostaining / in situ-hybridization-compatible Tissue hYdrogel (CLARITY) - cleared tissue. This enables imaging using standard fluorescent widefield or optical sectioning microscopies. Not only does our method uses less hazardous reagents, but the highly sensitive TPE-4TA also uses silver nitrate concentrations up to two million-fold lower than the standard Yamamoto-Hirano's modification of the Bielschowsky stain.

Paper III: Development of the novel near-infrared AIE fluorescent probe PM-ML with D-π-A (donor-pi-acceptor) structure for the selective staining of myelinated fibers in the teased sciatic nerves, mouse brain cryosections and $Clear^T$-cleared mouse brain tissue for 3D fluorescent imaging. We envision PM-ML as a potential tool for studying demyelination and evaluated its selectivity, photostability and signal-to-background (SBR) ratio which outperformed common commercial fluorescent myelin staining dyes.

List of scientific papers

I. **Fluorescent Silver Staining of Proteins in Polyacrylamide Gels.**

Wong AYH, Xie S, Tang BZ and Chen S.
Journal of Visualized Experiments. 2019. (146).

II. **Fluorescent Silver-AIE Visualization of Neurons and Fibres in the Cleared Brain.**

Xie S.*, **Wong AYH***, Chuen K, Hermanson O, Ip N, Tang BZ and Chen S.
Manuscript.

III. **A Near-Infrared AIE Fluorescent Probe for Myelin Imaging: From Sciatic Nerve to the Optically Cleared Brain Tissue in 3D.**

Wu MY*, **Wong AYH***, Leung JK, Kam C, Wu KLK, Chan YS, Liu K, Ip NY and Chen S.
Proceedings of the National Academy of Sciences of the United States of America. 2021. 9;118 (45), e2106143118.

*Authors contributed equally

List of related works not included in this thesis

I. **Fluorogenic Ag^+-Tetrazolate Aggregation Enables Efficient Fluorescent Biological Silver Staining.**

Xie S, **Wong AYH**, Kwok R, Li Y, Su H, Lam J, Chen S and Tang BZ. *Angewandte Chemie, 130 (20), pp.5852-5855*.

II. **Fluorogenic Detection and Characterization of Proteins by Aggregation-Induced Emission Methods.**

Xie S, **Wong AYH**, Chen S and Tang BZ.
Chemistry – A European Journal, 2019. 25 (23), pp.5824-5847.

III. **AIE molecular probes for biomedical applications.**

Wong AYH, Wang F, Kam C, and Chen S.
Aggregation-Induced Emission (AIE), 2022. pp.449-488.

IV. **Fluorescent Silver Staining Based on a Fluorogenic Ag^+ Probe with Aggregation-induced Emission Properties.**

Kam C, Xie S, **Wong AYH** and Chen S.
Handbook of Aggregation-Induced Emission, 2022. pp.541-558.

Contents

List of abbreviations

2D	Two-dimensional
2PE	Two-photon excitation
3D	Three-dimensional
ACQ	Aggregation-caused quenching
AIE	Aggregation-induced emission
AIEgen	Aggregation-induced emission luminogen
AIEE	Aggregation-induced emission enhancement
BABB	Benzyl Alcohol Benzyl Benzoate
BSA	Bovine Serum Albumin
CARS	Coherent anti stokes Raman scattering
CBB	Coomassie brilliant blue
CLSM	Confocal laser scanning microscopy
CPu	Caudate putamen
DiD	1,1'-dioctadecyl-3,3,3',3'-tetramethylindodicarbocyanine, 4- chlorobenzenesulfonate salt
DiI	1,1′-dioctadecyl-3,3,3′,3′-tetramethylindocarbocyanine perchlorate
DiO	3,3-dioctadecyloxacarbocyanine
DLS	Dynamic light scattering
DMSO	Dimethyl sulfoxide
DOPC	2-dioleoyl-sn-glycero-3-phosphocholine
DPBS	Dulbecco's phosphate buffered saline
DDPD	*N*, *N*-dicyclohexyl-1,7-dibromo-3,4,9,10-perylenetetracarboxylic diimide
DSPE-PEG2000	1,2-Distearoyl-sn-glycerol-3-phosphoethanolamine-*N*-[methoxy(polyethene glycol)-2000]
FITC	Fluorescein isothiocyanate
FFPE	Formalin fixed paraffin embedded
GFAP	Glial fibrillary acidic protein
GFP	Green fluorescent protein

HPS	Hexaphenlysilole
LDR	Linear dynamic range
LLD	Lowest limit of detection
LLS	Laser light scattering
LSFM	Light sheet fluorescent microscopy
MPPS	1-methyl-1,2,3,4,5-pentaphenylsilole
MS	Mass spectrometry
mSPIM	Multidirectional selective plane illumination microscopy
NADH	Nicotinamide adenine dinucleotide phosphate
NIR	Near infrared
OCM	Optical coherence microscopy
PBS	Phosphate buffered saline
PDI	Polydispersity Index
PDT	Photodynamic therapy
POPC	2-oleoyl-1-palmitoyl-snglycero-3-phosphocholine
RA	Retinoic Acid
RI	Refractive Index
RIM	Restriction of Intramolecular motions
RIR	Restriction of intramolecular rotations
RIV	Restrictions of intramolecular vibrations
ROS	Reactive oxygen species
S	Singlet state
S_0	Ground state
S_1	First electronically excited singlet excited state
SDS	Sodium dodecyl sulphate
SDS-PAGE	Sodium dodecyl sulphate polyacrylamide gel electrophoresis
SCoRe	spectral confocal reflectance microscope
SPIM	Selective plane illumination microscopy
SWIR	Short wave infrared

THBDBA	10,10′,11,11′-tetrahydro-5,5′-bidibenzo[a,d][7]annulenylidene
THG	Third harmonic generation
TPE	Tetraphenylethene
TPETPADCM	2-(2,6-bis((E)-4-(phenyl(4'-(1,2,2-triphenylvinyl)-[1,1'-biphenyl]-4-yl)amino)styryl)-4H-pyran-4-ylidene)malononitrile
UV	Ultraviolet

1 Introduction

Fluorescence imaging is an important tool for biomedical applications, ranging from visualizing proteins, intracellular organelles, or processes in cell biology to large structures in tissue and whole organisms. Fluorescence imaging requires understanding the fundamentals of both fluorescence and microscopy. There are specific conditions for a variety of applications which can benefit different types of experiments, such as avoiding fluorophores excited by lasers in the UV region in live cell imaging or clearing and decolorizing large thick tissue. Fluorescent tools are important and meaningful as they can ultimately affect your research and results. Not all fluorescent probes are created equally. They each have different photophysical properties which are beneficial for certain applications. Besides fluorophore and microscope optics, sample preparation can also affect the quality of the image.

Clearing methods are chemical techniques that allow us to turn tissue samples transparent. They preserve spatial resolution at the sub-cellular level whilst keeping the sample intact, providing optical access from whole organs to entire mammals (1). One of the major challenges with imaging large samples is pairing clearing techniques with powerful fluorescent probes that can diffuse quickly whilst exhibiting high brightness with excellent photostability for long and repeated imaging.

Chemical probes are an attractive fluorescent tool for transparent tissue labelling, especially when genetic, toxin or viral-based tracers do not apply to human samples. They can offer a unique and robust strategy to scale fluorescent labelling for large volumes such as the human brain or at high throughput, especially when large staining volumes or high concentrations are required. Ideally, a suitable probe will diffuse quickly into the tissue and stain with a good contrast whilst maintaining a good signal over a long period. However, most conventional chemical fluorescent probes suffer from quenching when aggregated, which is known as aggregation-caused quenching (ACQ). This is because of the strong π-π stacking which is intensified at high concentrations and when in poor solvents. In contrast, aggregation-induced emission (AIE) is an opposite phenomenon where the aggregation is instead beneficial with a turn-on fluorescent emission. AIE luminogens (AIEgens) paired with clearing methods offer a new strategy for 3D imaging of intact animal or human tissue. We aimed to design AIE-based probes that are optimized for fluorescent volumetric imaging to visualize neurons and myelinated fibers in 3D.

1.1 Fluorescence

The term “fluorescence” was first coined in 1852 by physicist professor George Stokes at the University of Cambridge. He observed that ultraviolet (UV) light could cause the

colorless mineral calcium fluoride (CaF_2) to illuminate a bright blue emission of light of which the emission wavelength was always longer than the excitation wavelength. The difference in the emission and excitation wavelength band maxima is known as the Stokes' shift (2). This can be described by the Jablonski diagram (Fig. 1), a schematic representation of the different energy levels during the absorption and emission of light by a fluorescent molecule, which was developed by the academic Aleksander Jablonski.

Electron pairs have anti-parallel spins in their molecular orbits which cancel out their magnetic moment, in what is known as a singlet state (S). A fluorescent molecule (fluorophore) that is not excited by light is represented by the ground state (S_0) (3). When a fluorophore absorbs a photon (within femtoseconds), energy is transferred and it becomes excited to a higher state (S_1, S_2, S_n) as its outer electron is boosted to another orbital. Several vibrational levels exist within each excited state with S_1 being the lowest. Depending on the level of energy absorbed, the molecule can be excited to a higher state such as S_2 or change vibration levels. Fluorescence is observed when the excited molecule transitions from an excited state (S_1) to the ground state (S_0) by losing the energy initially absorbed from the photon. This is because the difference in vibrational modes is large enough between S_1 and S_0 thus the probability of internal conversion (a form of nonradiative decay occurring within picoseconds) from the first singlet state to the ground state is least preferred (4) .

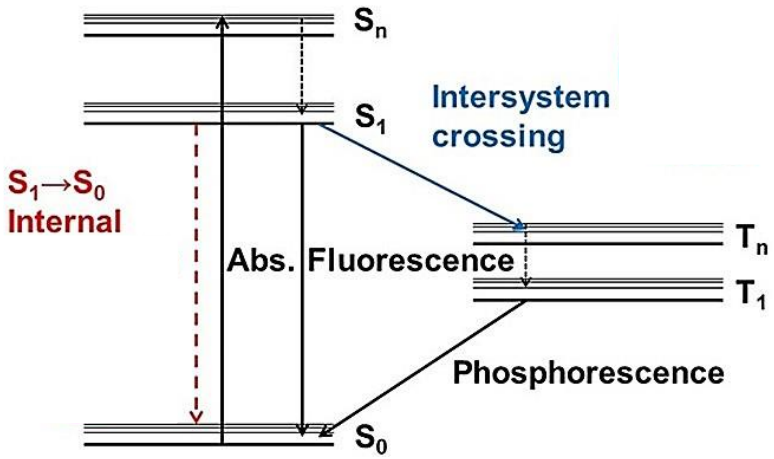

Figure 1: Jablonski Diagram. Simple illustration showing the excited states, vibration levels, non-radiative decay (internal conversion), fluorescence and phosphorescence emission. Modified with permission (5). Copyright 2020 John Wiley and Sons.

1.2 Fluorophores

There are generally three main types of fluorophores used in biological research: organic fluorophores, fluorescent proteins, and nanoparticles. The scientific community has been interested in the fluorescence of biological compounds since the development of the first fluorescence microscopes. Autofluorescence is derived from naturally occurring intrinsic fluorescent compounds which can be observed in cells, tissue, and other biological specimens. Intrinsic fluorophores include aromatic amino acids, flavins, NADH etc. (6).

Extrinsic fluorophores are synthetic or modified dyes that are added to samples for the detection of specific biomolecules such as DNA, proteins, or lipids where intrinsic fluorescence is absent. For this purpose, fluorescent probes with longer excitation and emission are preferred to avoid overlap with unlabeled biomolecules with intrinsic fluorescence.

1.2.1 Small Molecule Organic Dyes

Conventional fluorescent organic dyes can be typically characterized by their planar or cyclic structure, aromatic groups and π bonds which contributes to their highly conjugated structure. Small molecule organic probes are the most popular of the three main types of fluorophores, it is very easy to use and strategies from modern organic chemistry can be utilized to modify the dye's chemical structure, photophysical properties and function. Xanthene dyes such as rhodamine and FITC are the most widely used class of organic fluorescent dyes (Fig. 2). The most noteworthy conventional fluorophores are fluorescein and rhodamine, which have been popular for over a century and still serve as a platform for the development of sensors (7)

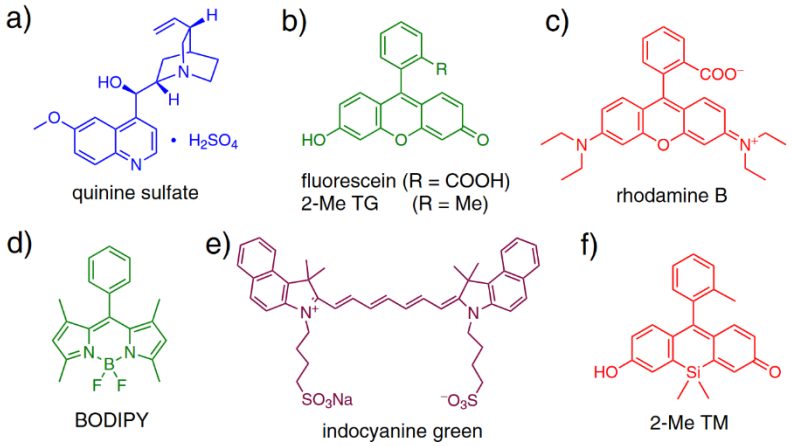

Figure 2: Representative examples of small organic fluorophores. a Quinine sulphate. **b,** Fluorescein and 2-Me TG. **c,** Rhodamine B. **d,** 1,3,5,7-tetramethyl-8-phenyl-BODIPY. **e,** Indocyanine green. **f,** 2-Me TM. The color of the dye represents the approximate emission color. Adapted with permission (8). Copyright 2013 Springer Nature.

1.2.2 Fluorescent protein

Fluorescent proteins are revolutionary tools, especially as genetically encoded tags, in cell biology and biochemistry. The wild-type green fluorescent protein (GFP) was isolated from the jellyfish *Aequorea victoria* by Osamu Shimomura in 1962 and has a molecular weight of 27 kDa comprising 238 amino acids. Thirty years later, Douglas Prasher succeeded in cloning the gene coding for GFP in 1992. GFP has a distinct 11 β-sheet barrel structure forming the walls and an α-helix running through the centre where the chromophore is protected, shorter α-helical "lids" are at each end of the barrel (9). The folding of GFP into the β barrel is important for forming the chromophore and the

fluorescence. The chromophore is matured (Fig. 3) by torsional rearrangement, intramolecular autocatalytic cyclization, and oxidation of the Tyr66 α-β carbon bond (10). The fluorescence is quickly produced shortly after transient expression in other organisms, and it can specifically tag proteins of interest in live cells (11) as the fluorescence can be preserved when fused with other proteins without significant adverse effects on its fused partner (12). The excitation and emission of fluorescent proteins can be optimized by random or site-directed mutagenesis. For GFP, this results in several variants with emissions ranging from 442 to 529 nm (13).

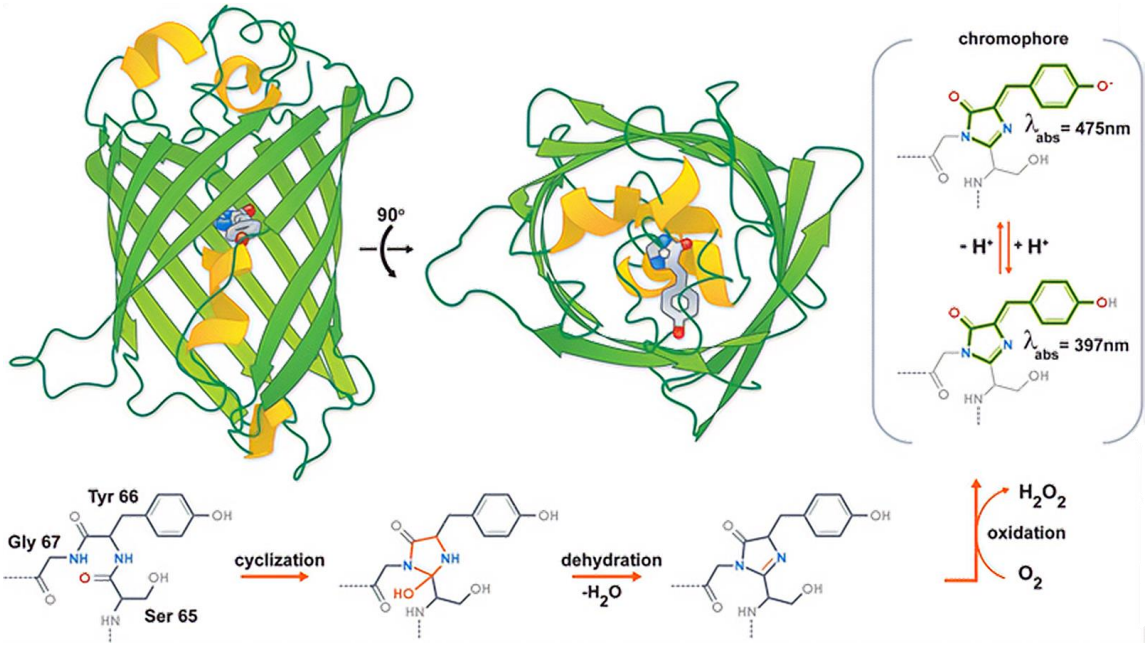

Figure 3: Maturation of A. Victoria GFP chromophore. Mechanism of the chromophore formation in GFP. Reproduced with permission (14). Copyright 2009 Royal Society of Chemistry.

Nowadays, hundreds of fluorescent proteins covering the spectrum from blue to far-red have been successfully isolated from different species or engineered. The small ultra-red fluorescent protein (smurfs) has been utilized for super-resolution imaging or as a fluorescence resonance energy transfer (FRET) sensor owing to its extreme photostability and being the brightest non-prototypical fluorescent protein (almost as bright as enhanced GFP). A bright and photostable red fluorescent protein is sought after for thick-tissue imaging in vivo (15).

1.2.3 Fluorescent nanoparticles

Nanoparticles (NPs) are commonly used in fluorescence imaging of biochemical species, cells, and tissues. There are a large variety of nanomaterials used for bioimaging, for example, fluorescent dye-doped silica nanoparticles, semiconducting polymer dots, AIE dots, carbon dots, quantum dots, gold nanoparticles and up conversion nanoparticles, etc. However, they lack specificity and response to ions and organic molecules unless modified. Targetability is achieved by functionalization through surface modification with

various ligands, for some nanoparticles hydrophilic surface molecules may be added to improve solubility (16). One of the main advantages of dye-doped nanoparticles over fluorescent small organic molecules is the stronger signal because a larger number of fluorescent dye molecules can be loaded into particles. The biocompatibility of nanoparticles has been debated, quantum dots are traditionally made of heavy metals which pose a serious concern to health and the environment. Toxicity may also arise because of impurities during synthesis. Furthermore, new green synthesis methods have gained popularity because of the safer and less hazardous procedure which can help reduce nanoparticle toxicity by using biocompatible solvents or phytochemical coatings (17–19).

1.2.4 Aggregation-caused quenching

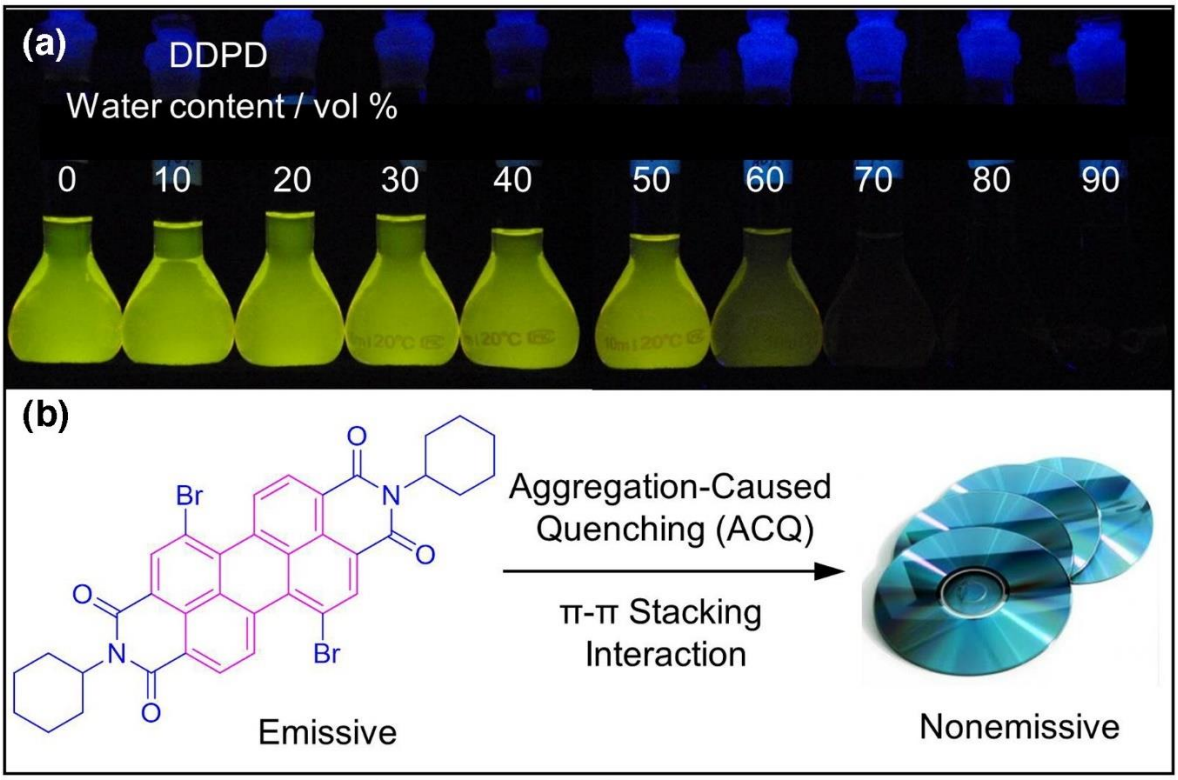

Figure 4: Aggregation-caused quenching (ACQ) phenomenon. a Photograph of the luminogen *N*, *N*-dicyclohexyl-1,7-dibromo-3,4,9,10-perylenetetracarboxylic diimide (DDPD) in different THF/water mixtures under UV irradiation. **b,** The molecular structure of DDPD molecules undergo ACQ due to intense π–π stacking interaction like stacked disks. Reproduced and adapted with permission from (20,21). Copyright 2009 Royal Society of Chemistry. Copyright 2015 Elsevier. License: CC-BY-NC-ND 4.0.

Conventional fluorophores are bright emitters as single molecules or in low concentrations. For example, fluorescein, like most conventional organic dyes is strongly emissive in solution or as isolated molecules. However, in concentrated solutions or the solid state, they can aggregate and lead to weak or fully quenched fluorescence. The intense π–π stacking interactions experienced by the aromatic rings of the aggregated fluorophore are responsible for this quenching effect (22). The excited state of these

detrimental excimers as aggregated molecules relaxes back down to the ground state via non-radiative channels (23) leading to quenching. *N*, *N*-dicyclohexyl-1,7-dibromo-3,4,9,10-perylenetetracarboxylic diimide (DDPD) is a hydrophobic molecule that displays a sharp decrease in fluorescence when aggregated in high water content mixtures and at high concentration (Fig. 4a). This is an example of a molecule that exhibits the ACQ phenomenon. DDPD favors the formation of excimers because of the highly aromatic and cofacial structure which prefer decay via non-radiative relaxation pathways (21).

1.2.5 Aggregation-induced emission phenomenon and fluorescent materials

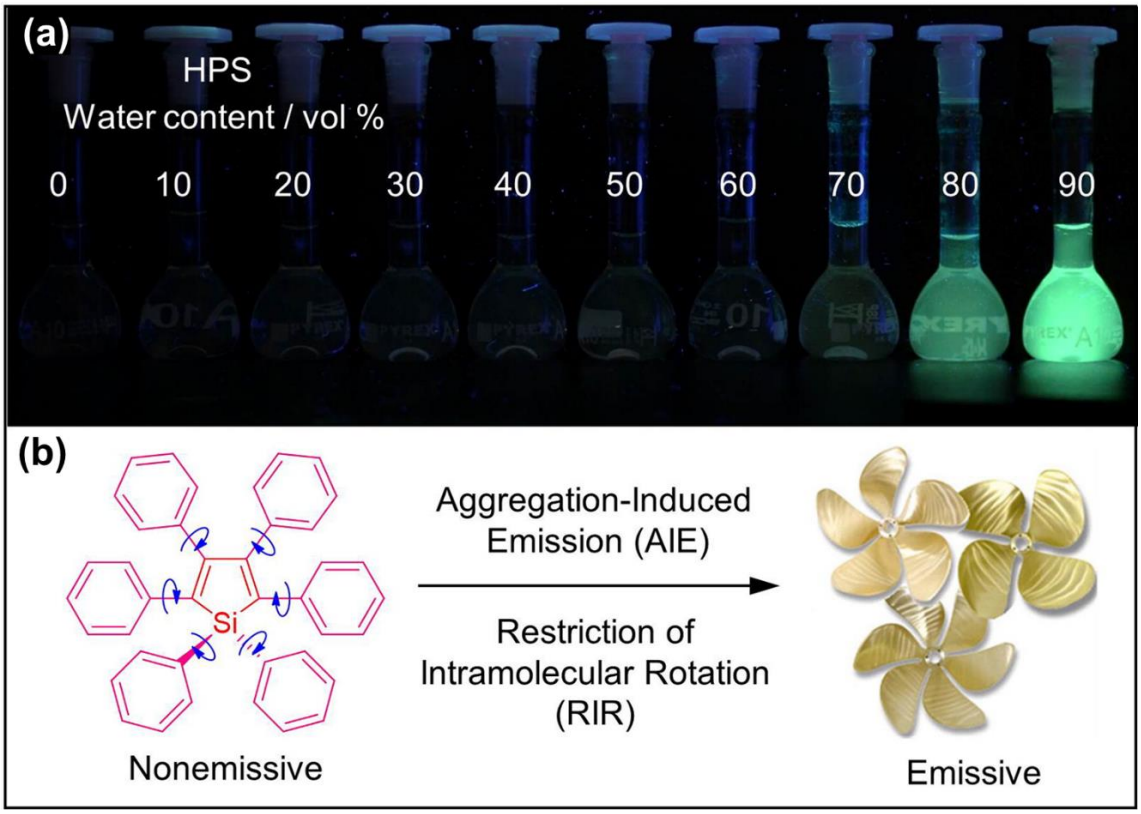

Figure 5: Aggregation-induced emission (AIE) phenomenon. a, Photograph of the luminogen hexaphenylsilole (HPS) in different THF/water mixtures under UV irradiation **b,** The molecular structure of HPS with multiple phenyl arms become restricted due to the restriction of intramolecular rotation (RIR) in the aggregated state leading to AIE. Reproduced and adapted with permission (20,21). Copyright 2009 Royal Society of Chemistry. Copyright 2015 Elsevier. License: CC-BY-NC-ND 4.0.

The phenomenon of aggregation-induced emission (AIE) was discovered in 2001 through the observation of 1-methyl-1,2,3,4,5-pentaphenylsilole (MPPS) in ethanol where fluorescence turn-on was triggered by water fractions above 50% (24). AIE has been described as the opposite of ACQ where it is weakly emissive in the molecularly dissolved state but fluorescently turned on in the aggregated state (22). It is a photophysical process that can be advantageous for biomedical applications. The aggregation-triggered emission may also serve to improve the signal-to-background ratio when staining cells or tissue as a turn-on dye as opposed to always on. With AIE luminogens, the efficiency of relaxation through internal conversion is affected by the restriction of intramolecular

motions (RIM) (5). The working mechanism of AIE is becoming clearer nowadays. RIM includes restriction of intramolecular rotations (RIR) and restriction of intramolecular vibrations (RIV). In RIR the rotations of phenyl rings in propeller-shaped molecules such as hexaphenlysilole (HPS) consume the excited-state energy through the non-radiative pathway resulting in no fluorescence emission when in the single molecule state (Fig. 5).

When the rotation is restricted in the aggregated state an enhanced "turn-on" emission can be observed. This phenomenon is not limited to molecules with rotatable bonds, an example of an AIE molecule with no rotatable aromatic rings rotors is 10,10',11,11'-tetrahydro-5,5'-bidibenzo[a,d][7]annulenylidene (THBDBA). This molecule can adopt the chair or boat conformation when fully solvated. The switching between the chair and boat conformation is the vibrational motion responsible for the absence of emission due to decay in excited-state energy. Phenyl ring torsion or double bond twisting leads to strong vibrational interactions between the S_1–S_0 electronic vibration levels upon excitation (25).

AIE luminogens (AIEgens) are very versatile fluorescent materials (Fig. 6) used for biomedical imaging. Not only can they specifically label structures of interest, but they can also be made into nanoparticles such as organic dots (AIE dot) for photodynamic therapy (PDT) to kill cancer cells or for deep tissue imaging (26). Some compounds exhibit a similar photophysical property to another phenomenon known as AIE enhancement (AIEE). The difference between a typical AIE and AIEE fluorophore is that the latter is still emissive as a single molecule but shows a significant fluorescent enhancement in its intensity in addition to a red shift in the emission spectra upon aggregation (27).

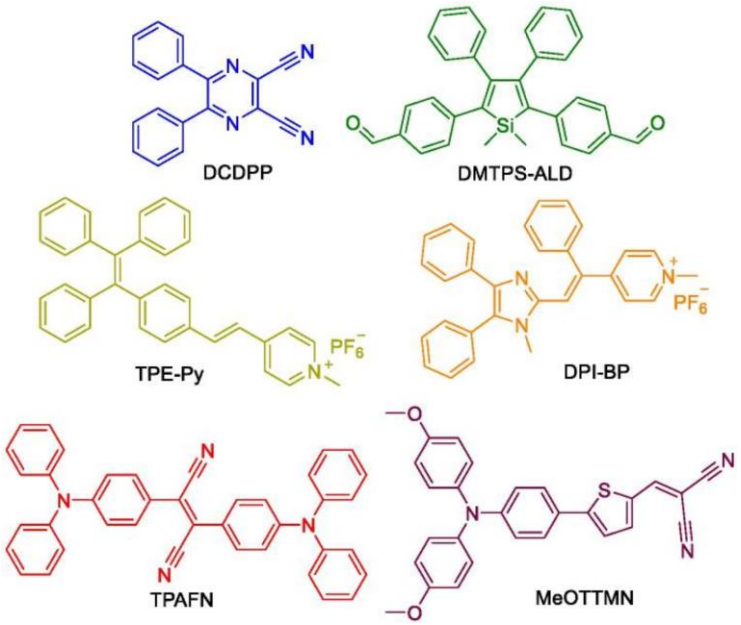

Figure 6: Typical examples of AIE luminogens. The color of the dye represents the approximate emission color from the whole visible range to the NIR range. Reproduced with permission (28). Copyright 2018 Ivyspring International Publisher. License: CC BY-NC 4.0.

Inorganic quantum dots, although bright with size-dependent emission, can exhibit low biocompatibility as they are often comprised of toxic heavy metal cores. Organic AIE dots, however, are a promising alternative for theranostics or bioimaging. AIE dots are nanoparticles with a dense AIE luminogen (AIEgen) as the core and encapsulated with a protective shell. AIEgens have a high loading capacity, leading to higher brightness. On the contrary, this would be difficult for most conventional ACQ dyes as they would likely quench from intense π-π stacking interactions (29). Theranostic applications of AIE dots have been utilized for image-guided photodynamic therapy (PDT). They can accumulate in tumors and generate reactive oxygen species (ROS) efficiently upon irradiation which leads to cell death by apoptosis. AIE dots have also been used for *in vitro* and *in vivo* long-term cell tracking.

The NIR dye 2,3-bis(4-(phenyl(4-(1,2,2-triphenylvinyl)phenyl)amino)phenyl)fumaronitrile (TPETPAFN**)** with an excitation peak (λ_{ex}) at 500 nm and emission peak (λ_{em}) at 660 nm (Fig. 7a) is an example of an AIE dot which has demonstrated such applications. Encapsulated with a mixture of Pluronic F-127 or lipid-poly (ethylene glycol) (PEG), 1,2-Distearoyl-sn-glycerol-3-phosphoethanolamine-*N*-[methoxy(polyethene glycol)-2000] (DSPE-PEG2000) or (Fig. 7b) and it has an amine end-capped variant DSPE-PEG2000-NH_2 allowing for functionalization by conjugation with the HIV-1 Tat cell-penetrating peptide (30).

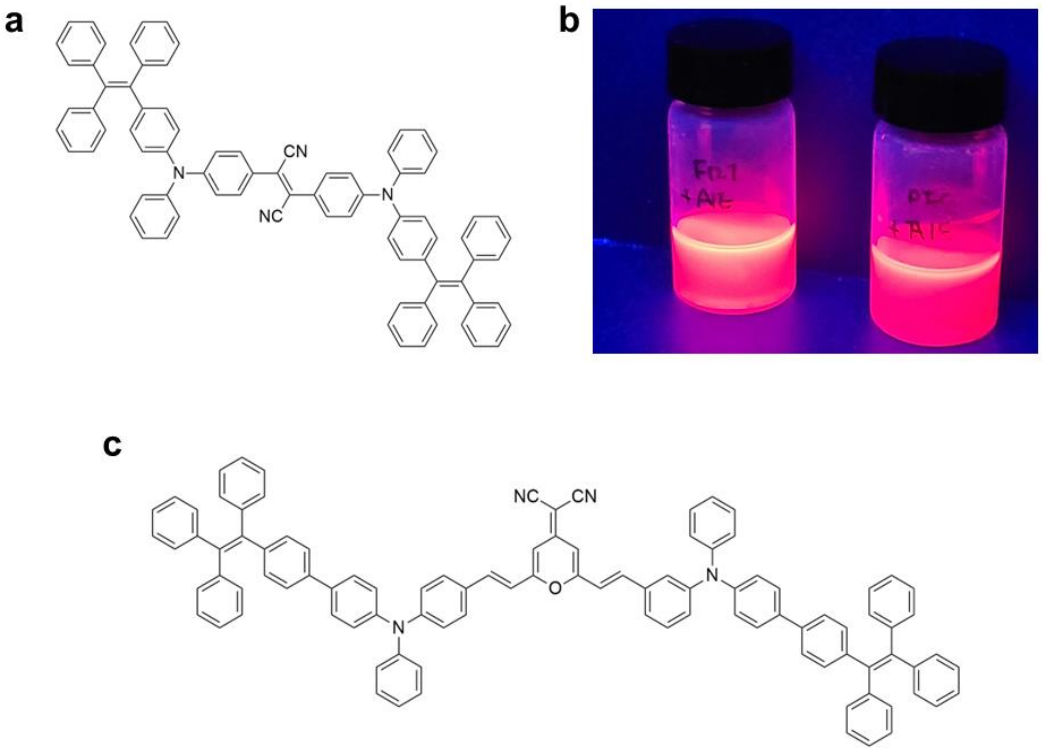

Figure 7: TPETPAFN loaded AIE dots. a, Chemical structure of TPETPAFN**. b,** TPETPAFN loaded into Pluronic F-127 encapsulated (left) and DSPE-PEG2000 (right) AIE dots. **c,** Chemical structure of TPE-TPA-DCM**.**

Other polymer matrices used for the fabrication of AIE NPs include the desolvation of bovine serum albumin (BSA) loaded with 2-(2,6-bis((E)-4-(phenyl(4'-(1,2,2-triphenylvinyl)-[1,1'-biphenyl]-4-yl)amino)styryl)-4H-pyran-4-ylidene)malononitrile (TPETPADCM) (Fig. 7c), which can be fabricated by traditional nanoprecipitation. AIE-based BSA nanoparticles have been shown to offer high biocompatibility and are being used for in vivo imaging of tumors (31). Qin & Tang *et al.,* 2012 also reported that the BSA NPs loaded with TPETPADCM had an average diameter of 307.3 nm however, it had a broad size distribution indicated by the polydispersity index (PDI) of 0.279 measured with laser light scattering (LLS) (30).

We demonstrated this method for other AIE dyes such as known as TPA-Alkyne (Fig. 8a) with a green emission (Fig. 8b) (32) encapsulated with BSA at a ratio of 1:1 and found that a more uniform and narrow size distribution could be achieved by a slow and gentle removal of THF through evaporation using compressed air for a minimum of 4 hours under a fume hood instead of rotary evaporation. Using dynamic light scattering (DLS) measurements, we show that the nanoparticles had a PDI of 0.071 and an average size of 60.1 nm (Fig. 8c).

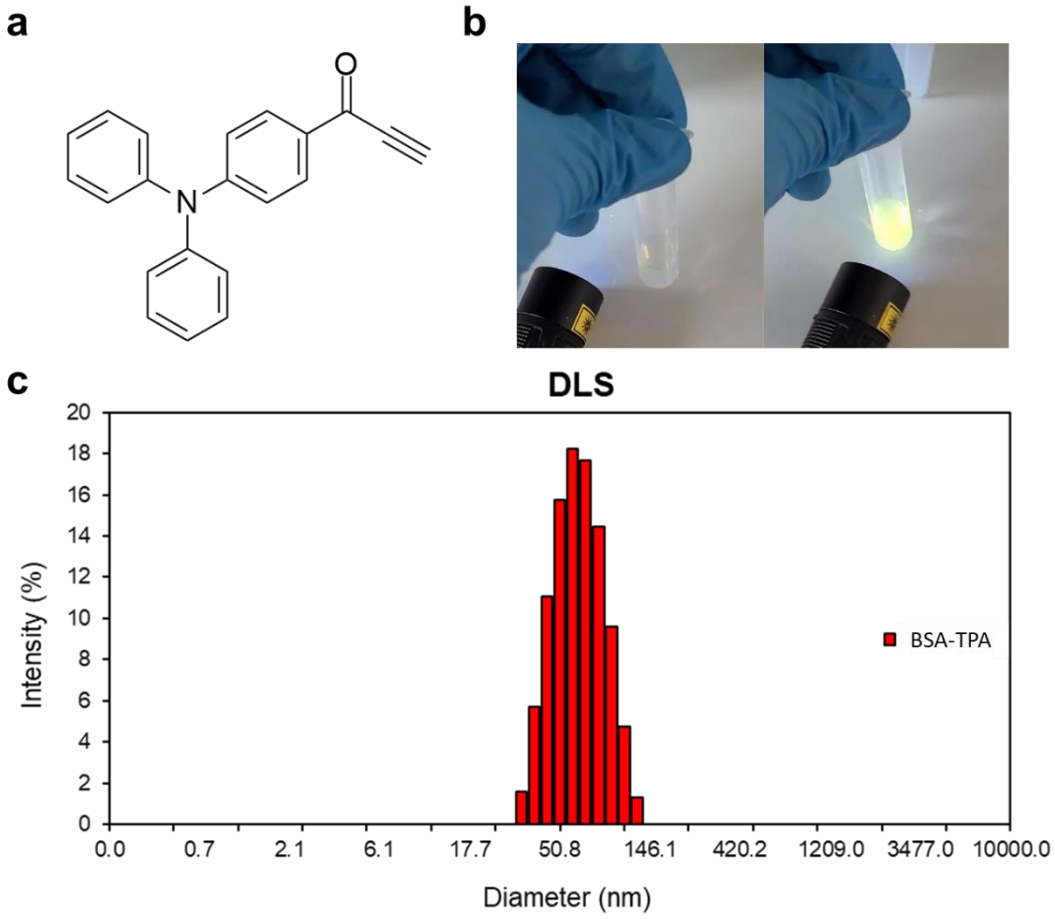

Figure 8: BSA-TPA nanoparticles. a, Chemical structure of TPA-alkyne. **b,** BSA-TPA nanoparticles before (left) and after (right) handheld UV illumination. **c,** The Size distribution of BSA-TPA nanoparticles in DMSO measured by dynamic light scattering.

1.3 Fluorescence Microscopy

Fluorescent widefield microscopes and slide scanners have been extensively used for imaging thin tissue sections. The entire volume of the sample is illuminated by excitation light and the structure of interest with the labelled fluorophores becomes excited and emits light of a longer wavelength. The light emitted from the sample is filtered and captured by a camera. Thick samples pose a challenge, the area above and below the focal plane is illuminated resulting in blurry and less resolved images. The poor resolution and image quality are also contributed by the light scattering caused by the lipids and proteins in the tissue, minimizing the diffracted light by RI homogenization of the tissue and mounting media can help alleviate this dilemma to an extent. With advanced microscopes, optical sectioning can allow us to illuminate only the focal plane of interest which can greatly improve the image quality and resolution in combination with clearing techniques. There are three main optical sectioning techniques (1) confocal laser scanning microscopy (CLSM), (2) two-photon excitation microscopy (2PE) and (3) selective plane illumination microscopy (SPIM) or light-sheet fluorescence microscopy (LSFM).

1.3.1 Confocal Microscopy

The confocal laser scanning microscope (single point) uses pinhole apertures in front of the light source and a second in front of the detector. The first pinhole focuses the illumination lights into a point of light on the sample by the objective lens. The emission light from the illuminated sample is then focused by the objective lens and into the pinhole before the detector which allows only the signal from the focal point to pass through and rejects the out-of-focus light from the detector (4). This is the main feature of a confocal microscope which was patented in the 1950s by Marvin Minsky. The complete image is built up of this diffraction-limited focal point scanned across the sample. The modern confocal microscope is composed of several fundamental components which include pinholes, objective lenses, excitation lasers, emission filters and detectors (33).

The optical sectioning offered by the confocal microscope allows the 3D reconstruction of a sample to be built up from stacks of images. Imaging large volumetric samples with a confocal can be challenging, this is because the illumination light passes through the sample before it reaches the focal point which can lead to photobleaching and photodamage before the plane of interest is imaged (34). Furthermore, the point-by-point scanning of the confocal is extremely slow, especially when combining tile-scans with z-stacks.

Besides single point laser scanning microscopes, multi point confocal (also known as spinning disk confocal) has unique benefits and drawbacks. For example, the spinning disk confocal has a higher imaging speed and lower light exposure, making it more suitable for live cell imaging. However, the pinhole is fixed and there is crosstalk when imaging at depth

due to multiple pinholes. This pinhole crosstalk can increase background signal in thicker tissue samples and ultimately diminishes the axial resolution (35).

1.3.2 Two-Photon Excitation Microscopy

The basic principle of two-photon microscopy is that the fluorophore is excited by the combination of two low-energy photons in a single event (within femtoseconds) from a pulsed laser (36). Each of these low-energy photons carries half the energy required usually needed in a single-photon absorption event. The wavelength of a photon is inversely proportional to the energy of a photon. In two-photon excitation, the wavelength of the photons is approximately double that of photons under one-photon excitation to achieve an equivalent transition. This means fluorophores can be excited by two photons in the infrared region over a single photon from the UV-visible range and still produce the same fluorescence emission.

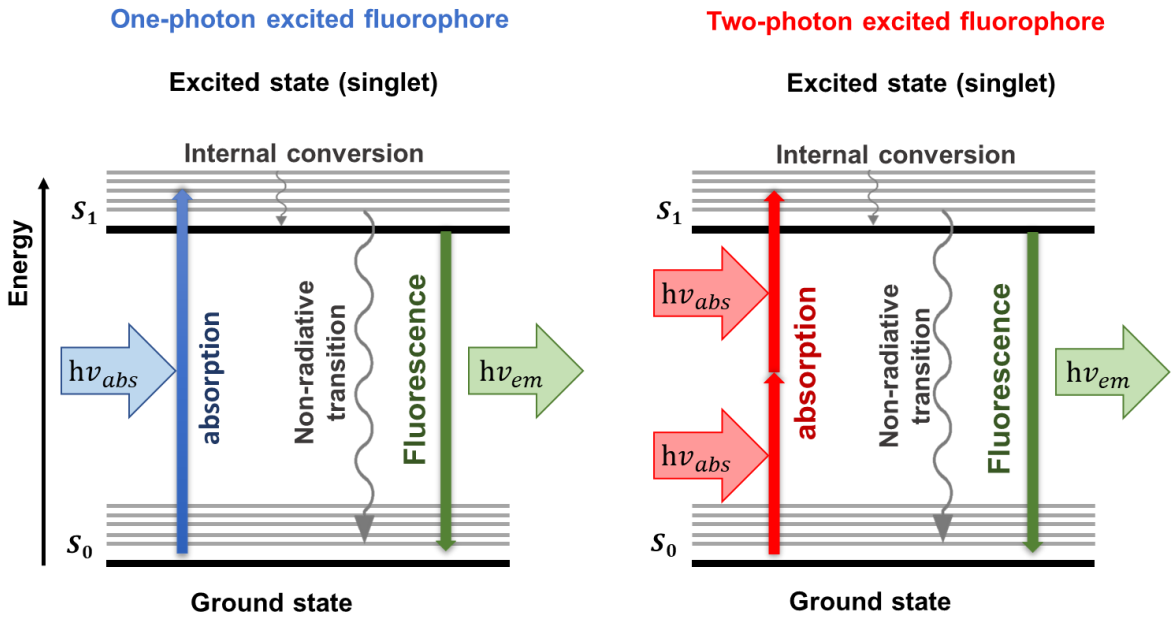

Figure 9: Jablonski diagram of one-photon and two-photon excited fluorescence. When a fluorophore absorbs one photon it produces fluorescence (left) simultaneous absorption of two photons of half the energy gap can produce the same fluorescence of the same wavelength.

This makes two-photon microscopy ideal for deep-tissue imaging, the longer excitation wavelength is advantageous in penetrating deep tissue with less scattering. Since two-photon excitation depends on the square of the excitation intensity, optical sectioning can be achieved by avoiding photobleaching outside of the focal plane. This is because the pulsed infrared light source and high NA objective focus the converging excitation light to a diffraction-limited spot at the focal plane where the photon density is greatest. This means the probability of two-photon interacting with the fluorophore simultaneously increases at the center of the focal plane and is significantly greater compared to outside of the focus. The lack of absorption outside the focus allows more excitation to reach the focus efficiently (37). Furthermore, the localized excitation in two-photon microscopy will

reduce the amount of background fluorescence even without a pinhole (Fig. 10) as the fluorescence is only emitted from the focal point. The chances of scattered photons reaching the fluorophore simultaneously outside the focus are practically none (37,38). For these reasons, two-photon imaging is ideal for volumetric imaging than confocal, especially when combined with clearing techniques. However, the 3D raster scanning of small focal points leads to slow and long acquisition times in confocal microscopy and two-photon microscopies.

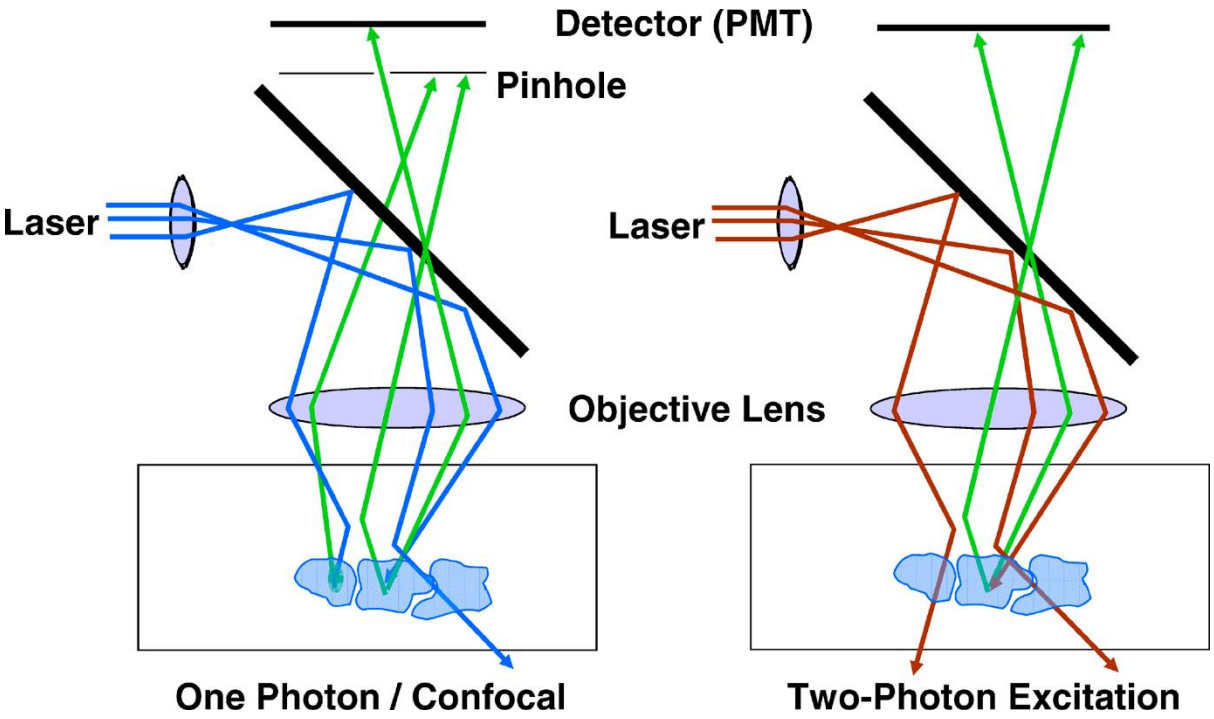

Figure 10: Diagram of light scatter in single and two-photon microscopy. Effect of scattering in confocal microscopy and two-photon excitation microscopy (38) Copyright 2005 David W. Piston Creative Commons Attribution License: CC BY-NC 4.0**.**

1.3.3 Selective Plane Illumination Microscopy

Selective plane illumination microscopy (SPIM) also known as light-sheet microscopy can provide optical sectioning for quicker high-resolution imaging with a large field of view whilst also being gentle on the sample in terms of photobleaching. In SPIM, the illumination and detection paths are decoupled. A thin sheet of excitation light illuminates only the observed plane within the sample avoiding the generation of out-of-focus fluorescence which provides optical sectioning with minimal photodamage. The illuminated plane is perpendicular to the imaging axis where fluorescence is collected and imaged (34). A higher axial resolution can be achieved over conventional fluorescence microscopy although this is limited to the thickness of the illuminated plane. A static light-sheet can be generated by focusing the excitation laser with a cylindrical lens. In the case of digitally scanned laser light-sheet fluorescence microscopy (DSLM), the light sheet is created through the rapid scanning of a collimated beam. This dynamic light-sheet produces a

more homogenous image and is less affected by light scatter than its static counterpart, therefore reducing image artefacts (39).

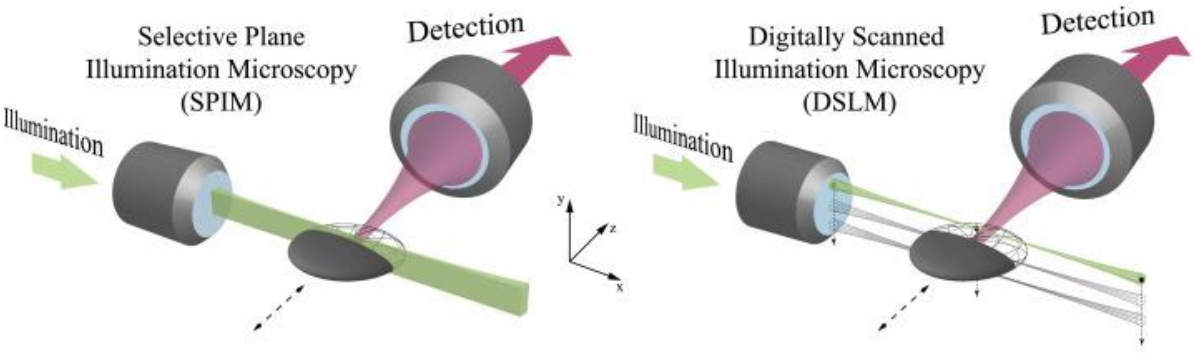

Figure 11: Diagram of SPIM and DSLM. SPIM excites the sample using a thin sheet of light generated through a cylindrical lens located at the back focal plane of the objective lens. In DSLM, the light beam is scanned along the detection focal plane at high speed, generating a virtual light sheet. Reproduced with permission (40). Copyright 2020 Elsevier. License: CC BY-NC-ND 4.0

Artefacts occur due to the scattering or absorption of light by impurities, air bubbles or pigmentation spots etc. Scattering is more prevalent in the living specimen where the refractive index is inhomogeneous, and absorption-related artefacts occur mostly in cleared tissue. Both scattering and absorption generate shadows with striping artefacts seen most intensely with single-side illumination although this can be reduced with dual-side illumination. There are many light sheet configurations which have partly addressed this issue by rotating the light sheet in multidirectional selective plane illumination microscopy (mSPIM) or using a confocal detection line in DSLM or more recently a combination of the two in multidirectional digital scanned light-sheet microscopy (mDSLM) architecture where angular diversity is improved by generating an elliptical Gaussian beam (41).

1.4 Tissue clearing

Thin slices cannot reveal the detailed 3D structure and microenvironment of cells and tissues. methods such as fluorescent micro-optical sectioning tomography (fMOST) which can reconstruct 3D images from serial slices are incredibly labor-intensive and time-consuming. The mechanical integrity of the ribbons of ultrathin slices cannot be guaranteed and the risk of knife artefacts and mechanical damage to the slices is high. Parts of the dataset can be ruined because of this, especially if there are missing slices. Making the tissue intact and transparent is a faster and less resource or labor intense approach to generating volumetric images (42).

To visualize biological structures in 3D at greater depths in a nondestructive manner the transparency can be manipulated. The amount of light scattering in the tissue needs to be reduced. As light travels through tissue it is scattered continuously with decay in

intensity as it is absorbed by endogenous molecules such as melanin or heme (43). Efforts to improve the transparency of tissue are focused on reducing light scattering and light absorption. This can be achieved in multiple ways, but the main goal is to homogenize the refractive index (RI) throughout the tissue to minimize the amount of diffracted light. Biological samples have a complex mixture of structures and macromolecules which causes this light scattering, making the tissue opaque. The color-absorbing pigment in tissue can also be reduced by bleaching with hydrogen peroxide (44). There are three general approaches (Fig. 12) to tissue clearing: solvent (hydrophobic), aqueous (hydrophilic) and hydrogel-based methods (45).

The first clearing method was invented by H. Lundvall in Sweden, 1905 to stain the skeleton of whole human embryos (46). Later, Werner Spaltzholz developed another clearing method using the organic solvent methyl-salicylate and benzyl-benzoate (47,48). It was elaborated later as methyl-salicylate was replaced by benzyl alcohol, this new mixture of benzyl alcohol and benzyl benzoate is known as Murray's clear (BABB) (49). The method was later further developed for 3D imaging of solvent-cleared organs (3DISCO) such as the whole mouse brain (50). The principles of hydrophobic clearing methods are centered around three steps: dehydration, delipidation and finally refractive index (RI) matching. The first two steps remove water and lipids, and the final step saturates the tissue with another liquid that has similar RI to water and further reduces light scattering. Organic solvent based clearing methods achieve the highest level of transparency in fixed tissues as demonstrated in the SHANEL method (51) which has been shown to clear entire intact human organs such as the brain.

The hydrophilic or aqueous based clearing methods use water soluble agents. A few examples include sucrose, dextran, urea, and amino alcohols which are less harsh and damaging to tissue while also highly biocompatible and relatively safe to handle. Different mechanisms are involved in these methods. They are generally passively immersed in RI matching solution or decolorized, delipidated and hyperhydrated. For example, urea is used in Sca/e (52) and amino alcohols in clear, unobstructed brain or body imaging cocktails and computational analysis (CUBIC) (53).

Hydrogel-based methods utilize the immobilization of amino groups containing biomolecules through crosslinking. Notable methods include the CLARITY (54) and passive CLARITY technique (PACT) (55). Acrylamide monomers are diffused into tissue and polymerized to form a hydrogel scaffold, anchoring proteins and other biomolecules. The detergent SDS is employed for dilapidation by passive shaking at or by electrophoretic transport. Crosslinking and tissue gelation can still occur without acrylamide monomers as demonstrated in SWTICH clearing (56) using glutaraldehyde. SWTICH utilizes "SWITCH ON" and "SWITCH OFF" buffers to inactive crosslinking or antibody labelling to achieve tissue homogenization before reactivating for uniform

staining. The use of a weaker SDS containing solution also allows for the delabelling of antibodies to achieve high multiplex imaging.

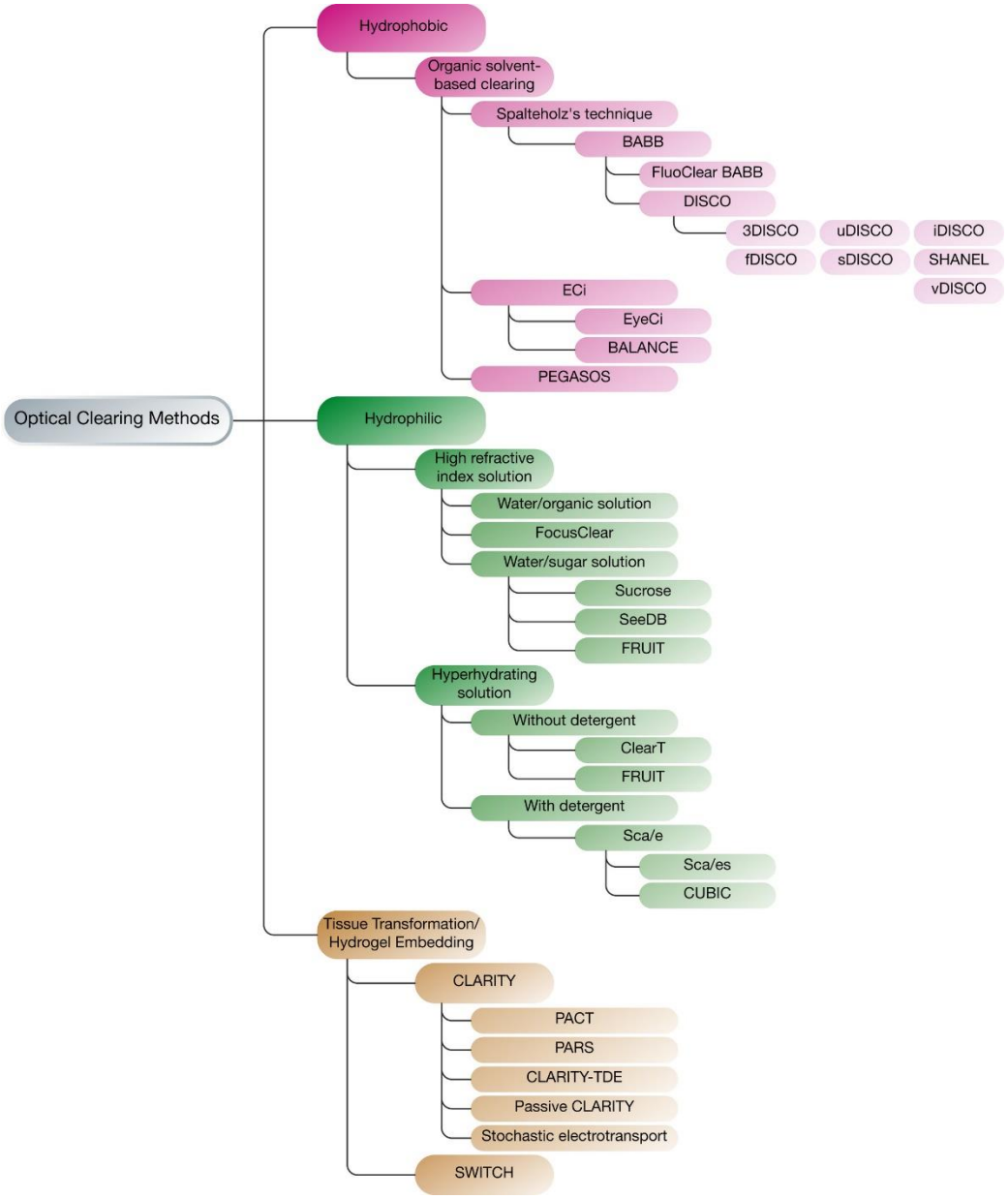

Figure 12: Tissue clearing methods derived from the three main categories. A tree diagram of common clearing method subtypes based on hydrophobic, hydrophilic, or hydrogel-based categories. Reproduced with permission (57). Copyright 2021 John Wiley and Sons under the CC BY 4.0 license.

1.5 Silver staining

The first reported silver nitrate staining for modern science application on fresh tissue was performed by Krause in 1844 for histological examination (58). Decades later, the emergence of a silver stain which could stain neurons and glia appeared in 1873 called The Golgi silver impregnation method. This method was invented by the Italian Professor of Histology and General Pathology Camillo Golgi (59). It was much needed at the time due to the poor resolution of tissue components when stained by hematoxylin and carmin

(60). The Golgi impregnation method was a revolutionary tool which was fundamental to other investigators, particularly Santiago Ramón y Cajal who made numerous modifications to Golgi's silver stain in additional to several new silver staining protocols with different silver development methods and "double impregnation" procedures (61). Golgi believed in the reticular theory that the nervous system was one single entity, as opposed to Cajal's neuron doctrine which stated that the nervous tissues were made up of discrete functional individual cells, the latter being the correct depiction. Gustav Retzius, a professor in histology in 1877 at Karolinska Instituet discovered a horizontal cell type from the human fetus using the Golgi method. Cajal also reported the same cell type in the rabbit which was later named Cajal-Retzius cell. Retzius' studies of the peripheral nervous system further supported Cajals neuron doctrine (62).

Both Golgi and Cajal won the Nobel Prize in Physiology and Medicine in 1906 "in recognition of their work on the structure of the nervous system (60)." The silver method proved to be popular with its versatility, as numerous new silver methods and modifications (some still being used today) could specifically visualize specific cell types or structures. An example is Cajal's pupil Rio Hortega, who created the ammoniacal silver carbonate method that allowed visualization of glial cells (61).

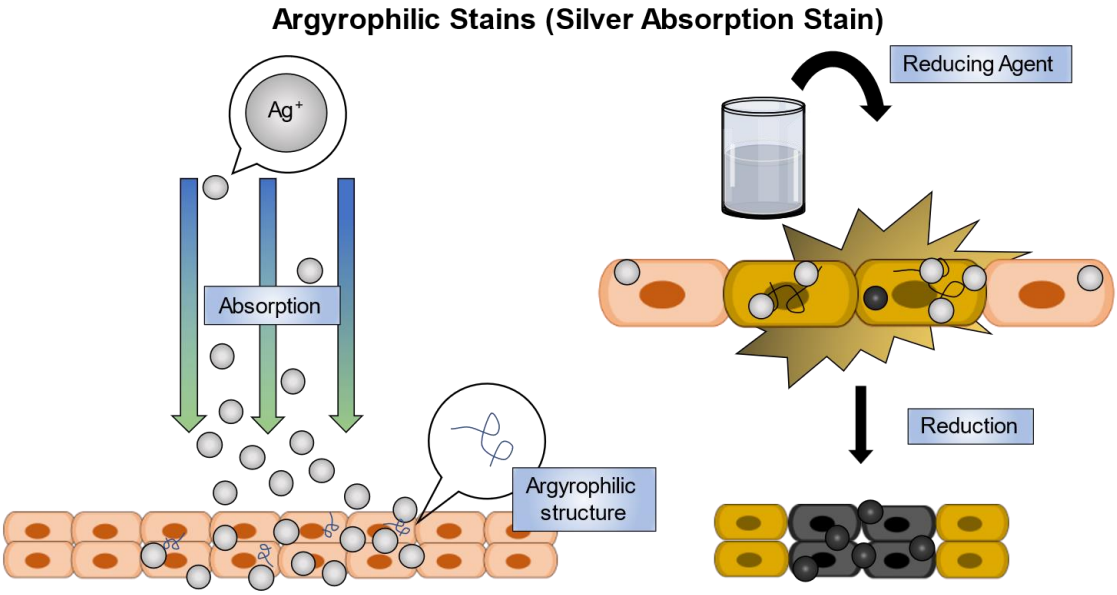

Figure 13: Schematic of a general argyrophilic staining mechanism. It is observed that certain "argyrophilic structures" in tissue or cells can rapidly absorb ionic silver in acidic or basic silver solutions. Exogenous reducing agents are added to reduce the absorbed ionic silver into metallic silver deposits.

Silver staining can be categorized into five general types based on their development into reduced silver. This includes silver absorption stains "argyrophilic" (Fig. 13) where certain biological structures can absorb silver ions (Ag^+) rapidly from silver salt solutions, eventually, this is visualized by adding an exogenous reducing agent to reduce Ag^+ into elemental silver. This can be further divided into basic, acidic, or neutral stains (63). The

histochemical mechanism for the argyrophilic reaction is yet to be determined, although studies have suggested that silver forms complexes with various side chains of amino acids. The imidazole nucleus is responsible for the formation of silver complexes in histidine which also acts similarly to the guanidyl group of arginine (64). Furthermore, Sulphydryl groups (also known as thiol groups) are well known to form compounds and interactions with a silver (64–67). Proteins that lacked the thiol-rich amino acid cysteine such as the 3500 Da hormone, glucagon stained negatively with silver in SDS-PAGE (67). An example of an argyrophilic stain is the "Grimelius stain" used to visualize granules in neuroendocrine cells (68,69). In principle, silver ions are readily absorbed by the granules in neuroendocrine cells and the unbound excess silver is washed away. The absorbed silver ions are then reduced into metallic silver grains by development with hydroxyquinone-sodium sulfite solution (63).

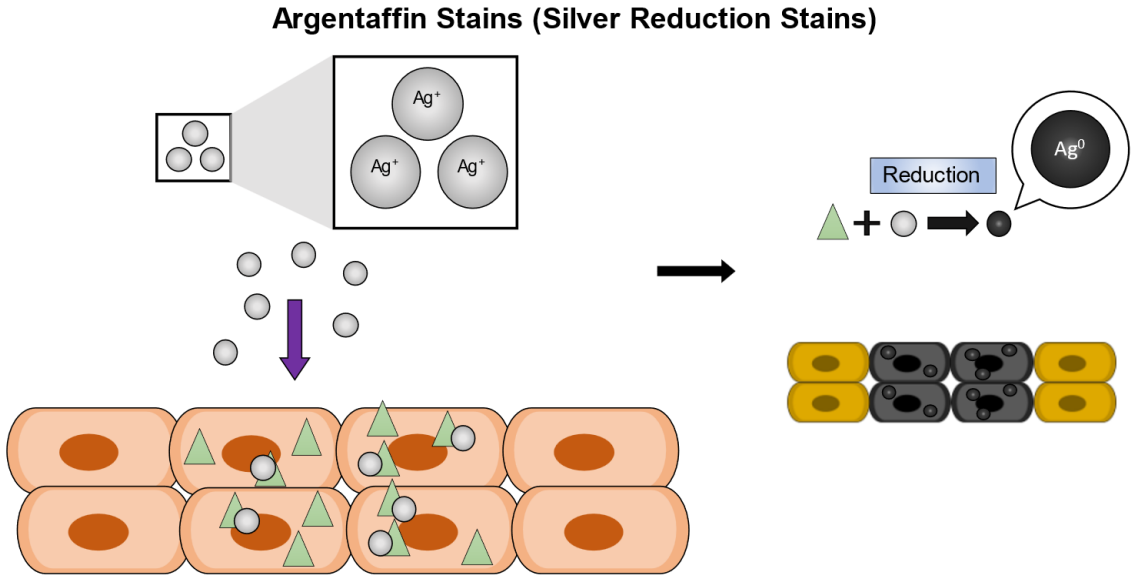

Figure 14: Schematic of a general argentaffin staining mechanism. Ionic silver in basic silver salt solutions deposit metallic silver at sites of reducing groups.

For the Argentaffin stains, the active reducing groups are already present within cells such as aldehydes. They immediately reduce silver ions into metallic grains upon entry into the cell. The left-over silver ions are subsequently washed away (Fig .14), the main point is that no external reducing agent is applied (70).

Silver oxidation-reduction stains also known as "combination stains" (Fig. 15), work by using strong oxidizing agents like chromic acid on carbohydrates and glycoproteins to convert cellulose-polysaccharides or chitin in the fungal walls to create new aldehyde-reducing sites. Applications include staining of fungal walls using the Gomori methenamine silver stain, however, there must be an adequate amount of oxidation otherwise there will be nonspecific poor-quality stains if an adequate amount of aldehyde groups are not generated. On the contrary, excessive amounts of oxidizers can lead to overstaining and loss of detail. The exact time of oxidation needs to be controlled as

aldehydes have argentaffin reactions, it can be beneficial to block existing aldehydes before the oxidation step.

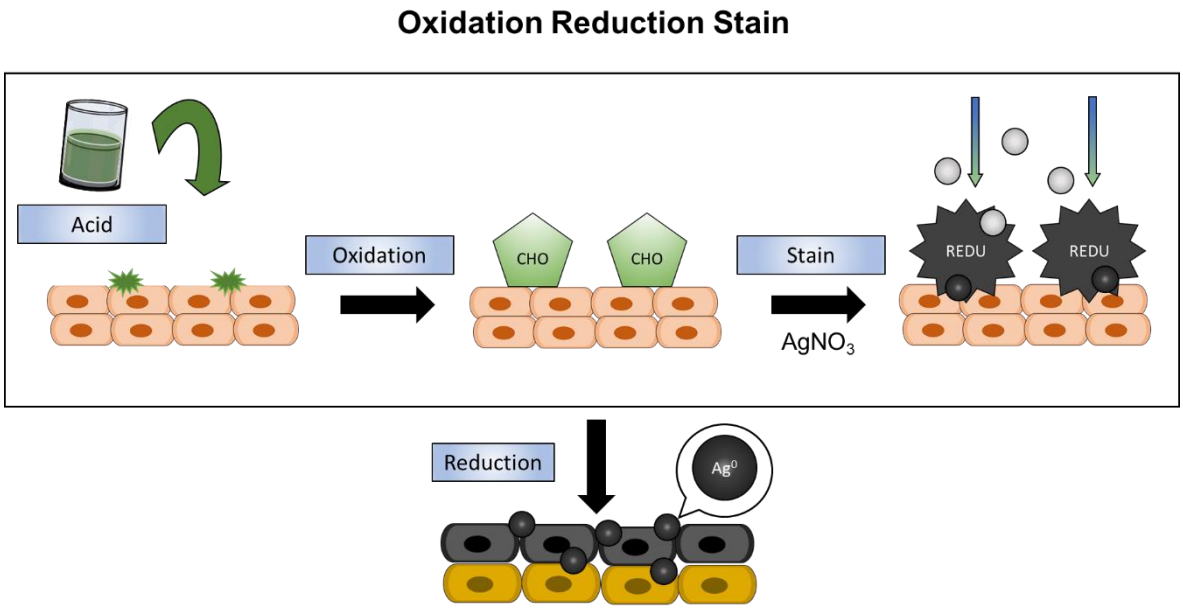

Figure 15. Schematic of a general oxidation Reduction stain. Strong oxidizing agents such as chromic acid are added to pre-treat the tissue to form reducing sites such as aldehydes. The tissue is then stained with silver which is subsequently reduced to metallic silver deposits at reducing sites.

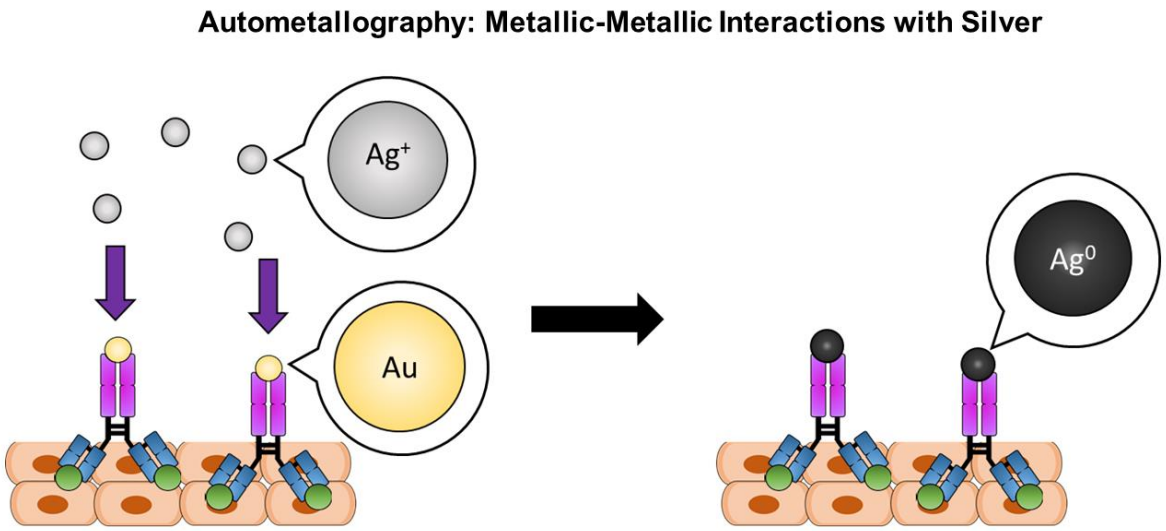

Figure 16. Metallic-Metallic Interactions with Silver. This method relies on the antibody-antigen interaction. Gold particles are conjugated to the Fc fragment, intensification occurs when silver forms a shell of metallic silver on the gold particles.

In metallic-metallic interactions (silver autometallography) silver is used for intensification of immunogold labelling which allowed adaptation for light microscopy (Fig. 16). After immunogold labelling, the added silver forms a shell around the gold particles. This method can also be used to amplify endogenous metal deposits like mercury, zinc,

and metallic silver in living tissue. Metals like gold and silver function as seeds, providing a large surface area to catalyze the reduction of ionic silver in the presence of a reducing agent such as hydroquinone. If the silver autometallography occurs for too long, the surface area of microparticles becomes too large, leading to a greater accumulation of silver deposits and precipitation causing high background staining.

1.5.1 Bielschowsky's silver stain

Bielschowsky's silver stain (Fig. 17) is a popular method amongst neuropathologists that is still being used today. This method was modified from the Fajersztajn method which was almost forgotten (61). Fajerztajn's method first demonstrated the impregnation of frozen sections to visualize cylinder axes using ammoniacal silver oxide. The main mechanism of these methods is derived from the chemistry used to make mirrors, which uses the ammoniacal silver diamine $[Ag(NH3)2]^{+}$ complex to form the silver mirror. This is also similar to Tollens' reagent which creates the silver mirror upon the detection of aldehydes. Max Bielschowsky modified Fajersztajn's method by adding a silver impregnation step before the main ammoniacal silver impregnation with formalin-fixed frozen sections. It is suggested that is additional silver step provides foci for silver deposition in the ammoniacal silver solution. Bielschowsky's stain has been modified for the paraffin section, the Yamamoto-Hirano's modification is generally accepted as the standard protocol for clinical neuropathological examination of human brain samples.

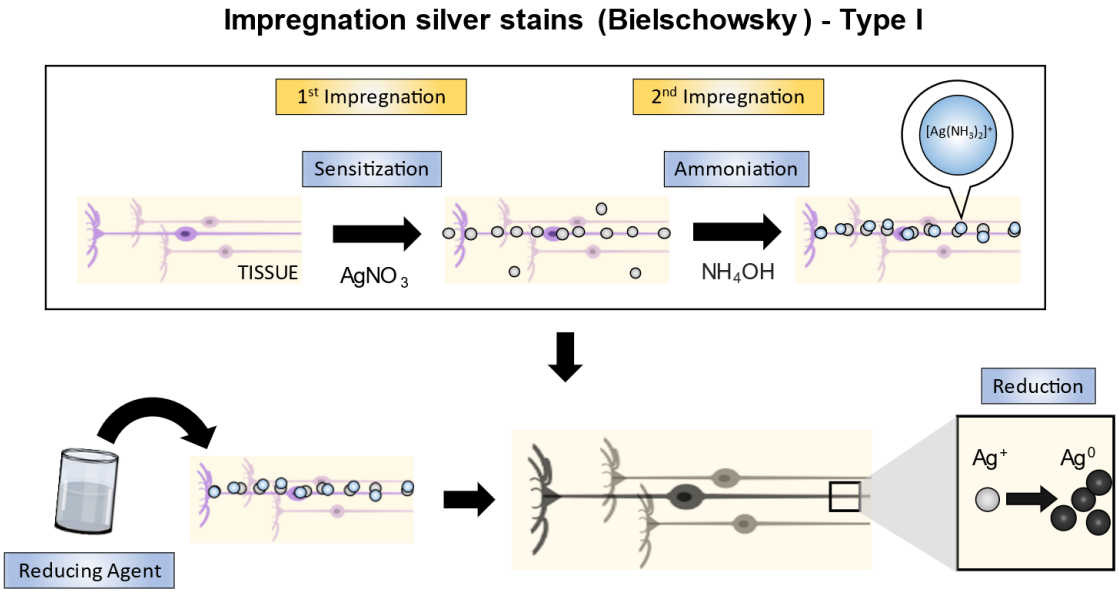

Figure 17. Bielschowsky Silver stain. The tissue section is first sensitized with a silver nitrate solution, providing foci for silver deposition in the ammoniacal silver. A developer containing a reducing agent is used to visualize the section.

It is commonly used to visualize myelinated nerve fibers, neurofibrillary tangles, and amyloid and neuritic components of senile plaques (71). This modification differs from

others because of a second ammoniacal silver bath. Formaldehyde is added for silver development.

1.5.2 The Golgi silver impregnation method

The Golgi stain, also known as the black reaction (reazione nera) required the tissue to be fixed and hardened by 5% potassium dichromate (slow variation) and osmium (for the rapid Golgi stain) before impregnation in a 0.5-0.7% silver nitrate bath for several days (61). This allows for the crystallization of silver chromate on the surface of the plasma membrane spreading to the inside of the neurons (72) (Figure 18).

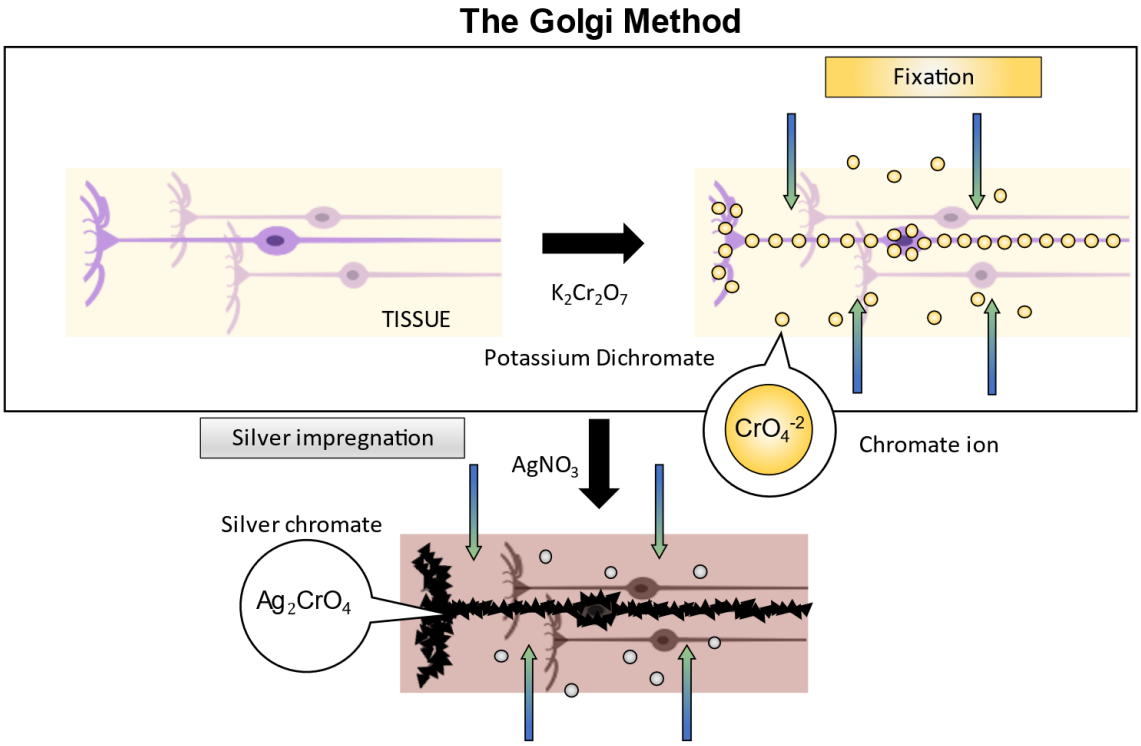

Figure 18: Illustration of the Golgi staining mechanism. The tissue is fixed with potassium chromate for several days and after a 0.5% silver nitrate wash it is bathed in 0.5-0.7% silver nitrate solution which eventually crystallizes into silver chromate.

The Golgi stain has been superseded by its modified variant "Golgi-Cox" which uses mercuric chloride and potassium dichromate with potassium chromate. The chromium salt binds to the proteins of cells, the black mercury deposit is the transformation of the whitish mercury chloride into mercury sulfide by alkalization. The tissue sample needs to be hardened so that it can be sectioned into thin slices for light microscopy, the optimal thickness has been reported to be 200 microns thick for studying dendritic arborization (73). The limitations of the Golgi stain have hindered its use with advanced microscopy, studies have shown that both the traditional Golgi and Golgi-Cox stain can be combined with the tissue clearing "CUBIC" and stain other structures with fluorescent probes such as amyloid plaques using Thioflavin-S. However, the Golgi silver-stained neurons are not fluorescent and can only be visualized by brightfield light microscopy, the silver stain in

this case does not take full advantage of the confocal microscope for fluorescent imaging (74). Other attempts have been reported to bring the Golgi staining method and other metal-impregnated stains to advanced microscopy, by a phenomenon known as surface plasmon resonance which can reveal 3D cytoarchitecture. Imaging is performed using spectral fluorescence microscopy to collect emissions shorter than the wavelength of the laser excitation. However, for a standard non-spectral CLSM additional optical filter sets would need to be procured from the manufacturer.

1.6 Fluorescent Silver Probes

Metallic silver itself has been shown to directly exhibit fluorescence under specific conditions. Ag_2S quantum dots can produce fluorescence at different wavelengths. The absorption and emission wavelength increases due to the growth of the Ag_2S core nanocrystal from excess sulfur, which is a unique optical property of QDs, the size-dependent luminescence is known as the quantum size effect (75). With the addition of a silica-coated shell, Ag_2S/SiO_2 can extend into the near-infrared whilst maintaining water solubility and a hydrodynamic diameter of less than 10 nm (76). Furthermore, it has been reported that a fluorescence "turn on-off" can be observed in polyethyleneimine-capped Ag_2S QDs interaction with heparin, the relevance is that the effect is mediated by AIEE (27,77).

Metallic silver such as silver chromate in the Golgi method has been reported to fluoresce through a phenomenon known as surface plasmon resonance, where the emission wavelength is shorter than the excitation laser wavelength. This allows the visualization of the 3D cytoarchitecture in existing traditional Golgi-stained samples. However, this method requires non-standard optical filter sets to capture the emission wavelengths shorter than the excitation laser. If the CLSM could not be configured to detect up-conversion, a spectral detector would be needed (78). Silver can also be detected in the ionic state, chemosensors are often developed as an off-on probe to detect Ag^+ in the environment and for bioimaging.

1.6.1 Silver ion sensors

Silver ions bind to various metabolites, and proteins and can inactivate enzymes, it is harmful to aquatic organisms (79,80), silver and various silver complexes are also toxic to algae, fungi, and bacteria. The detection of silver ions can be divided into three main categories depending on the sensing mechanism and platform used: 1. coordination-based systems, 2. reaction-based systems, and 3. other materials and systems (which include quantum dots, nanoparticles, polymers, and oligonucleotides) (81). An example of coordination-based system is rhodamine B Selentone (RBSe). It is a sensor for Ag^+ and Hg^+ and works by exploiting selenium's strong affinity for these ions by incorporating a Se atom into the spirocyclic structure of rhodamine. The selenium atom forms a complex with the silver ion; this complex is separated by hydrolytic cleavage of the selenoactone

bond leading to the release of rhodamine B and fluorescence revival (Fig. 19). This probe showed a detection limit of 58 nM for Ag^+ (82). However, the turn on mechanism would leave the dye unbound to the silver ion and may not be suitable for bioimaging.

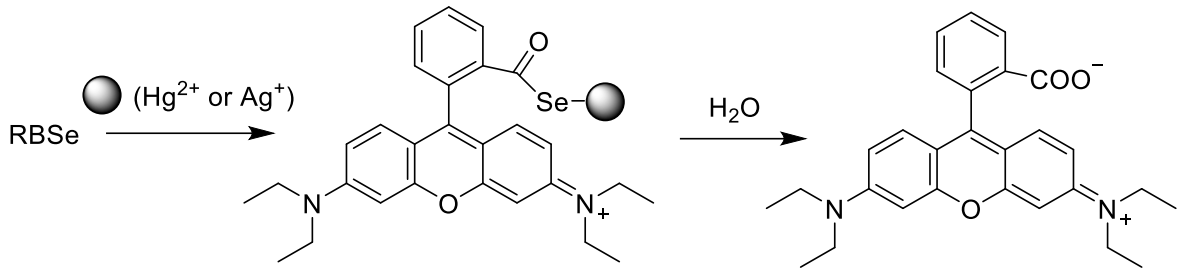

Fig. 19: Scheme of RBSe reaction mechanism. Adapted with permission (82). Copyright 2010 American Chemical Society.

A fluorescent probe that would be suitable for detecting silver bound complexes in bioimaging would be one that exhibits high sensitivity, photostability and can be applied at high concentrations without the risk of quenching. One of the first AIE silver ion sensors based on tetraphenylethylene (TPE) was developed by Liu *et al*. in 2008 which exploited the specific binding of adenine (compound 1) and thymine moieties (compound 2) for Ag^+ and Hg^+ respectively (Fig. 20) with an emission band at 470 nm for Ag^+ with a detection limit of 0.34 μM (83).

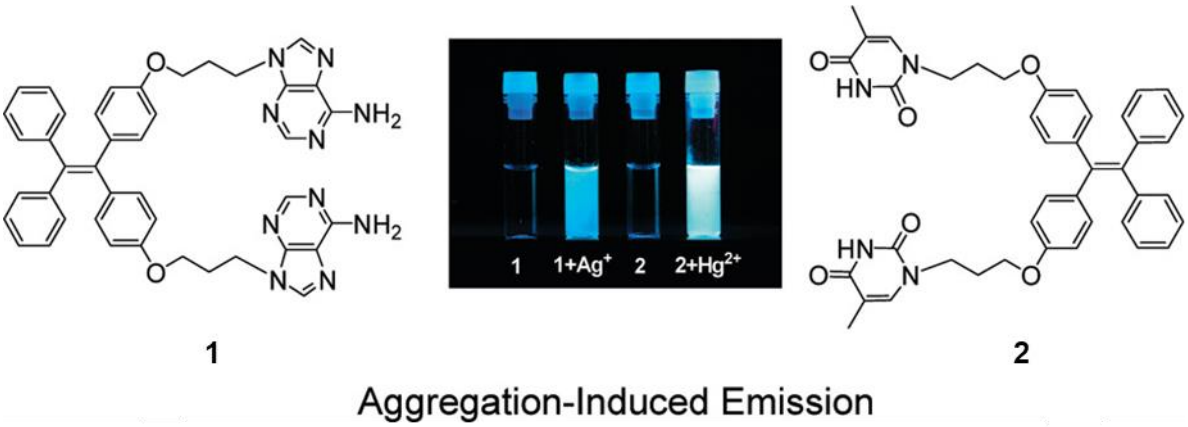

Fig. 20. Structure of Ag+ and Hg+ sensitive compounds 1 and 2 with adenine and thymine moieties. Reproduced with permission (83). Copyright 2010 American Chemical Society.

1.7 Neuroimaging based on chemical fluorescent staining

Neuronal tracers are important for the understanding of local neural circuits amongst a web of seemingly infinite connections. It is estimated that the human brain has an average of 86 billion neurons and 85 billion non-neuronal cells (84), chemical probes would be a preferred method to stain large volumetric samples of human tissue. Due to limited choices of small molecule probes, imaging tools in neuroscience are mostly dominated by methods using genetic manipulation to encode sensors (85,86). Fluoro-gold is a neuronal tracer with the active constituent of a weak base hydroxystilbamidine that

involves retrograde transport. It is proposed that Fluoro-gold crosses the membrane and enters acidic organelles such as lysosomes and endosomes, leading to the trapping of bases in Fluoro-gold in these compartments (87). Fluorescent Nissl stains can visualize neurons using commercial dyes like NeuroTrace™ or cresyl violet (88) which are often used as a counterstain as chemical probes are often combined. Some probes are degenerative stains that are specific to pathological hallmarks like amyloid-β (Aβ) fibrillar aggregates like Thioflavin T (89) or injured degenerating neurons like Fluoro-Jade (90).

Probes that can stain live and fixed neurons include lipophilic carbocyanine dyes such as 1,1′-dioctadecyl-3,3,3′,3′-tetramethylindocarbocyanine perchlorate (DiI). They are also anterograde and retrograde neuronal tracers. It can be applied to the neurons by various means, for example as a crystal using the tip of a glass microcapillary tube or microinjection using a Picospritzer. Lipophilic carbocyanine dyes can also reveal details of microstructures such as dendritic spines. Being limited by slow diffusion speed and compatible with only aqueous-based RI homogenization methods, lipophilic carbocyanine dyes are inferior to a highly thermal stable dye that enables fast diffusion and is compatible with a variety of clearing methods requiring delipidation (91).

1.8 Fluorescent probes for myelin labelling

Myelination facilitates the propagation of electrical impulses along axons in saltatory conduction. Commercial dyes such as FluoroMyelinTM Red/Green are reported to label myelin in brain tissue sections and cultured Schwann cells by incorporating into the myelin sheaths (92). Lipophilic carbocyanine such as DiI, 1,1'-dioctadecyl-3,3,3',3'-tetramethylindodicarbocyanine, 4- chlorobenzenesulfonate salt (DiD) and 3,3-dioctadecyloxacarbocyanine perchlorate (DiO) can not only label cell membranes and trace neuronal connections and vasculature but also label the myelinated fiber tract. DiO has been demonstrated to stain myelinated fiber tracts in the striatum of cleared tissue sections (93). There are many label-free methods to visualize myelin in vivo, this includes optical coherence microscopy (OCM), third harmonic generation (THG) and spectral confocal reflectance (SCoRe) microscopy, and coherent anti-Stokes Raman scattering (CARS) (94). SCoRe is the most accessible platform among these methods as it utilizes a standard confocal microscope without using complicated specialized equipment in the other methods. However, SCoRe is reported to have difficulties in resolving myelinated axons travelling in the z-axis (95). It is desirable to visualize the myelinated fiber tracts in the cleared brain with a good signal-to-background ratio, high photostability, and long storage shelf-life since a large amount of the staining solution would be needed for large samples and it may also take some time to image the whole specimen. Tissue clearing also homogenizes the RI in the sample to mitigate light scattering. It is unclear whether this could compromise the use of SCoRe in cleared tissue which is based on differences in RI between the lipid-rich myelin and the axon.

2 Research aims

The overall aim of the thesis work is to develop fluorescent chemical probes for neuroimaging and optimize the staining performance in cleared tissue for three-dimensional imaging. The specific aims of the three projects are as follows:

I. In paper I, the aim is to develop and investigate the performance of a new fluorogenic silver staining protocol for SDS-PAGE using the novel water-soluble AIE probe TPE-4TA as a fluorescent protein gel stain.

II. In paper II, the aim is to adapt the fluorescent silver-AIE stain combined with immunofluorescence to visualise neurons in the mouse brain using formalin-fixed paraffin-embedded (FFPE) tissues and in 3D with PFA-fixed intact tissues cleared by passive CLARITY.

III. In paper III, by using the AIE-based near-infrared probe PM-ML, we aim to develop a new myelin-specific staining method in cryo-sections, PFA-fixed sciatic nerves and cleared tissues using the Clear^{T} method for 3D visualisation.

3 Materials and methods

The materials and methods used in paper I-III are briefly described here. Please see the attached papers for further details. Ethical permits were obtained by the collaborators.

3.1 Gel electrophoresis

The PageRuler™ Unstained Protein Ladder was purchased from Thermo Fisher Scientific. It contained a mixture of 14 recombinant proteins ranging from 10–200 kDa. The unstained ladder was loaded into 1.0-mm-thick NuPAGE™ 4–12% Bis-Tris protein gels (Invitrogen). The first lane was loaded with double volumes of the ladder stock (10 µL) followed by the normal stock volume (5 µL) in the second lane and a series of two-fold dilutions of the stock thereafter (13 dilutions, from twofold to 8192-fold) spanning a total of 15 lanes. The dilution was performed by mixing Milli-Q water (18 Ω), NUPAGE™ sample buffer and NUPAGE™ sample reducing agent (Invitrogen). Each stock had a protein concentration of 20–50 µg/µL in the buffer (62.5 mM Tris-H_3PO_4, pH 7.5 at 25°C, 1 mM EDTA, 2% SDS [sodium dodecyl sulfate], 10 mM DTT, 1 mM NaN_3, 0.01% bromophenol blue, and 33% glycerol). SDS-PAGE was performed with NuPAGE™ MES (2-[N-morpholino]ethanesulfonic acid) SDS Running Buffer using the Mini Gel Tank (Invitrogen) at a constant voltage of 200 V for 30 min with the PowerEase® 300W power supply (Thermos Fisher Scientific). SYPRO™ Ruby Protein Gel Stain (Thermo Fisher Scientific) was performed following the manufacturer's protocol.

3.2 Silver nitrate gel stain

The silver stain was performed using the protocol reported by Jin et al. (96). Following electrophoresis, the gels were first fixed for 1 h in a 40% methanol/10% acetic acid (HAc) solution and then rinsed in 100 mL of ultra-pure water for 3 × 10 min. Next, the gels were impregnated with 100 mL of 0.2% (w/v) silver nitrate solution for 20 min in a sealed glass container. Afterwards, the gel was washed with 100 mL of Milli-Q water for 2 × 15 s. Finally, the gel is developed in 100 mL 3% (w/v) sodium carbonate and 0.046% (v/v) formaldehyde (1.25 mL, 37% formaldehyde/L). Development was terminated by washing in 100 mL 1% HAc solution repeatedly. The silver gels were imaged by an Azure c600 gel documentation system.

3.3 Fluorescent silver-AIE gel stain

After electrophoresis, the gels were fixed in a 40% ethanol/10% HAc solution for 2 × 30 min on a shaker at 50 rpm, then rinsed in 100 mL of ultra-pure water for 3 × 10 min. Next, the gels were impregnated with 100 mL 0.0001% $AgNO_3$ solution at room temperature for 1 h. Afterwards, the gel was washed twice with 100 mL of ultra-pure water for 1 min and transferred to a new container with 100 mL of TPE-4TA fluorogenic staining solution (10 µM) on a shaker for 12 h or 2 h at 60°C. In the final washing step, the gel was transferred

to a new container with 100 mL destaining solution (10% ethanol) for 30 min. After a quick rinse in water, the gels were imaged by an Azure c600 gel documentation system at 302 nm or 365 nm UV channel.

3.4 Animal samples

Fixed animal samples were obtained from The Hong Kong University of Science and Technology (Hong Kong, China) and The University of Hong Kong. Animal sacrifice is approved by the Animal Ethics Committee (HKUST: A19053, A18042; HKU: CULTAR 4704-18) which was carried out following respective institutional guidelines that also conform to international guidelines.

3.5 Paraffin sectioning

Fixed C57BL/6J mouse brains were dehydrated sequentially in ethanol, and xylene, and infiltrated with paraffin wax using a tissue processor (ThermoFisher, Excelsior™ AS Tissue Processor). Processed brains were then embedded in paraffin wax using the Thermo Scientific Shandon Histocentre 3, sectioned to 8 μm with a microtome (Leica, RM 2235S), and mounted onto slides.

3.6 Immunofluorescence co-staining

The procedure for achieving dual immunofluorescence labelling and silver-AIE staining involved several steps. First, the brain section was permeabilized and blocked using a mixture of 0.025% Triton X-100, 3% bovine serum albumin, and 0.3 M glycine for 1 hour at room temperature. Afterwards, the section was incubated with a recombinant Alexa Fluor 647-conjugated anti-NeuN antibody at (Abcam; ab190565) 4 °C overnight. The slides were then rinsed with PBS and the stained sections were fixed with 4% PFA for 1 hour.

Following this, the slides were washed three times in ultrapure water for 5 minutes each to remove any residual PBS or PFA. The section was then ready for the silver-AIE staining of FFPE tissue sections.

3.7 Silver-AIE staining of FFPE brain sections

First, FFPE tissue sections were deparaffinized twice in xylene for 5 min each, twice in absolute ethanol, twice in 95% ethanol, twice in 75% ethanol, twice in 50% ethanol, and thrice in ultra-pure water (18.0 Ω) for 3 min each. Then, each section was placed in 50 mL of 0.005% silver nitrate solution (Acros Organics) buffered with 0.01 M borate-boric acid buffer, pH 8.0 diluted from the addition of 0.1M sodium tetraborate decahydrate (J&K Scientific) into 0.1 M boric acid (Sigma Aldrich) until the desired pH was reached (97). Silver impregnation was performed in a Coplin jar for 16 h at 37°C in the dark. Next, the tissue section was washed thrice in ultrapure water for 3 min

each. Afterwards, 15 µl of 26–30% ammonium hydroxide (J&K Scientific) was added dropwise (5 µl each) to the new silver solution for the second silver impregnation which was performed for exactly 5 min. Finally, the tissue section was washed thrice in ultrapure water for 3 min each and placed in 50 mL of 10 µM **TPE-4TA** overnight in the dark for fluorescence development. After washing, the tissue section was dehydrated in ethanol and xylene before mounting. DPX (dibutyl phthalate polystyrene xylene) mounting media (Sigma-Aldrich) was used to mount a No. 1.5H glass coverslip (Paul Marienfeld).

3.8 Passive clarity tissue clearing

3.8.1 Hydrogel preparation

The hydrogel solution was prepared on ice by mixing 20 mL of 40% (w/v) acrylamide solution (Bio-Rad), 2.5 mL of 2% (w/v) bis-acrylamide solution (Bio-Rad), 20 mL of 10× phosphate-buffered saline (PBS), pH 7.4 (Sigma-Aldrich), 0.5 g of 0.25% (w/v) VA-044 (J&K Scientific), and 157.5 mL of distilled water. The entire process was kept in the dark where possible and stored at -20°C for later use.

3.8.2 Embedding and polymerization of hydrogel-tissue

1-mm-Thick sectioned tissues or whole mouse brains were placed in a conical tube containing 50 mL of hydrogel solution for 3 or 7 d respectively at 4°C. The conical tube was then placed in a desiccation chamber with the lid unscrewed for gas exchange. The chamber was purged with nitrogen gas, vacuumed, and finally purged again. The lid was immediately screwed back on limiting exposure to atmospheric air and sealed with paraffin wax. The conical tube was then incubated in a water bath at 37°C for 3 h to initiate the polymerization of the hydrogel. Afterwards, the excess hydrogel was removed gently by using Kimwipes®.

3.8.3 Passive tissue clearing

A clearing solution containing a mixture of 0.2 M of boric acid and 80 g of SDS (4% w/v) was prepared. The pH was carefully adjusted to 8.5 by adding 1 M NaOH. The sample was placed into a 50 mL falcon tube with 20–50 mL of clearing solution at 37–55°C on a shaker for 3–14 d depending on the tissue size. The clearing solution was replaced every 1–2 d. After clearing, the samples were washed with 0.01% Triton X-100 in 0.01 M borate-boric acid buffer, pH 8 twice a day at room temperature, followed by an overnight wash in 0.01 M borate-boric acid buffer, pH 8 and a final change of buffer solution. The sample was stored at 4°C until subsequent staining.

3.9 Fluorescent silver staining of clarity cleared tissue

TPE-4TA was dissolved in ultra-pure water to make a stock solution of 1 mM. 5 µl of 1 M sodium hydroxide (NaOH) was added each time with a total of 15 µl and the stock solution was vortexed. The CLARITY-cleared tissues were impregnated with 50 mL of 0.00001% silver solution buffered in 0.01 M borate-boric acid buffer, pH 8.0 at 15 rpm for 24 h and washed in ultra-pure water for 30 min. The samples were then prepared and submerged in a second silver impregnation for a total of 3 h on a shaker. Finally, the cleared tissue was developed in 10 µM TPE-4TA buffered with 0.01 M borate-boric acid, pH 8.0 overnight for at least 12 h. An overview is illustrated (Fig. 21)

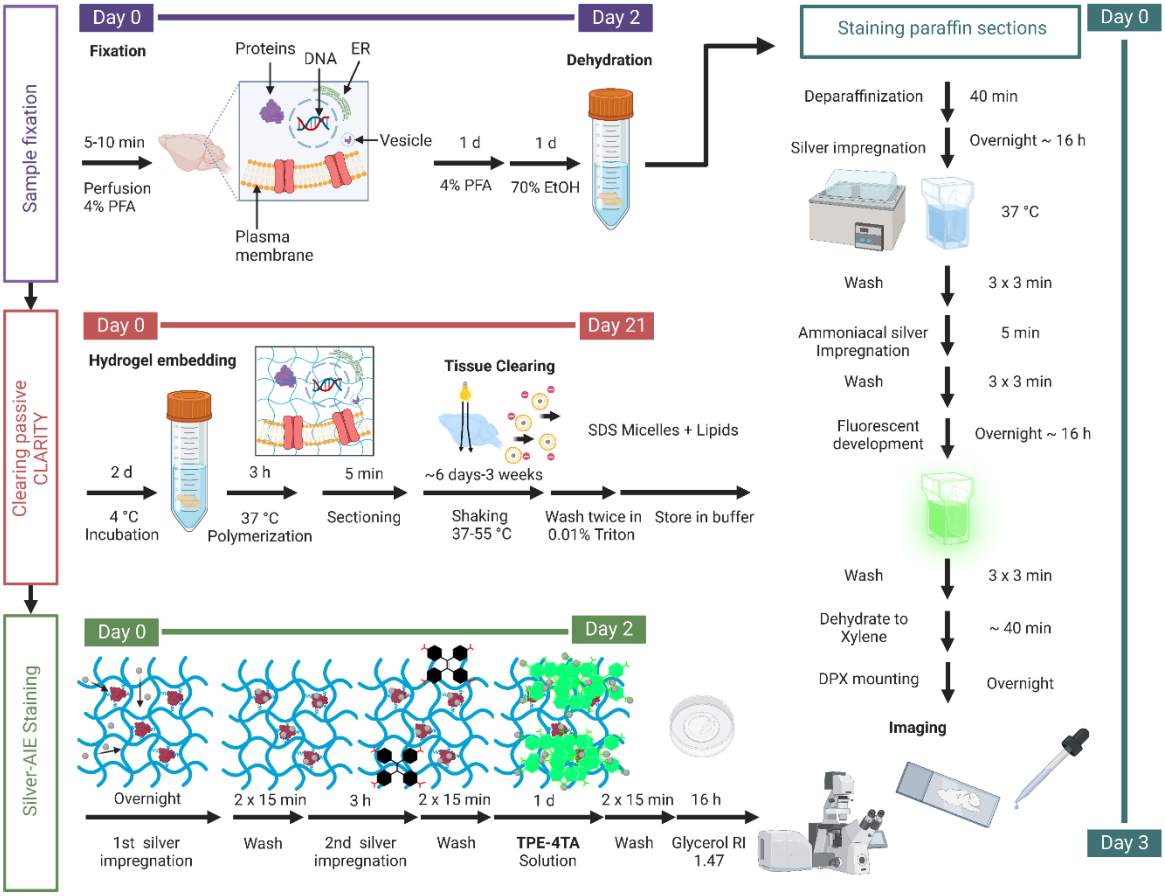

Figure 21. The fluorogenic silver-AIE staining pipeline. The fluorogenic silver method can be applied in fixed samples which can then be processed for paraffin 2D staining or passive CLARITY clearing before being impregnated with silver nitrate and stained with the TPE-4TA dye. Made in biorender.com.

3.10 Cryosections

The mice's brain was dissected and post-fixed in paraformaldehyde (PFA) at 4°C for 24 h. It was then sequentially immersed in 30% (w/v) sucrose (Sigma-Aldrich) in PBS overnight and a 1:1 mixture of 30% (w/v) sucrose with the O.C.T. (optimal cutting temperature) Compound (Tissue-Tek, Sakura Finetek USA INC.) for 24 h. After embedding

into the O.C.T. Compound for another 24 h, it was cryosectioned at a thickness of 12 µm with a CryoStar™ NX70 cryostat (Thermofisher) and adhered onto an adhesion glass slide.

3.11 Clear^T clearing

The clearing was performed using the Clear^T or Clear^{T2} method described. In the Clear^T method, the mouse brain was sequentially incubated in 20%, 40%, 80%, and 95% (v/v) formamide (J&K Scientific) in PBS (Sigma-Aldrich) or Dulbecco's phosphate-buffered saline (DPBS), pH 7.4 (Invitrogen) for 5 min each before incubating in a new solution of 95% formamide for 15 min. In the Clear^{T2} method, the mouse brain was sequentially incubated in 25% formamide (J&K Scientific)/10% PEG 8000 (polyethene glycol 8000; Sigma-Aldrich) in H_2O for 10 min and 50% formamide/20% PEG 8000 in H_2O for 5 min before incubating in a new solution of 50% formamide/20% PEG 8000 in H_2O for 15 min.

3.12 PM-ML myelin staining

3.12.1 Staining of cryosections

10 µM PM-ML in 10% (v/v) dimethyl sulfoxide (DMSO) in PBS/DPBS was prepared for staining of cryosections. A hydrophobic barrier was drawn around the sample and 200 µl of the PM-ML staining solution was dropped. Next, the cryosection was gently washed in PBS/DPBS and mounted with Fluoromount-G (Invitrogen).

3.12.2 Clear^T tissue staining

Thick (1 mm) tissue sections were added to a 50 mL falcon tube containing 30 mL of 1 µM PM-ML solution in 10% DMSO. Next, the section was washed with PBS/DPBS three times at 5-min intervals and then stained for 1–2 d. Finally, it was rinsed with PBS/DPBS before clearing.

3.13 Image acquisition and processing

Samples were imaged using the Nikon Eclipse Ci upright widefield microscope, the Zeiss LSM 880 confocal microscope, the Zeiss Light sheet 7 selective plane illumination microscope, the Nikon A1R HD25 confocal microscope, the Leica TCS SP8 MP two-photon microscope, BioTek Cytation 5 for slide scanning and the LiToneXL Light-sheet microscope. Images were processed and analyzed in ImageJ. This included temporal color coding, intensity profile plots including plane brightness and stack contrast adjustments for visualization. NIS-Elements Advanced Research was used for colocalization analysis and denoising. Zeiss Apeer was also used for denoising and segmentation. 3D visualizations were rendered on Imaris viewer.

4 Results and discussion

4.1 Paper I: Fluorescent Silver Staining of Proteins In Polyacrylamide Gels

Finding a novel fluorescent probe to stain neurons may require high-throughput screening of sensors from a combinatorial library (98) with a brain cell screening platform. We hypothesize that using our silver-sensitive AIE probe TPE-4TA, fluorescent labelling of biological targets can be achieved by silver nitrate staining. By creating a new fluorogenic silver staining method for proteins separated by SDS-PAGE, the low silver nitrate concentration and fluorogenic development in our silver method could mitigate the drawbacks of traditional silver techniques by reducing background, improving linearity and reproducibility.

Camillo Golgi and Santiago Ramón y Cajal demonstrated that silver could be used to visualize neurons in detail, it was not until the 1970s that silver staining was applied to polyacrylamide gels to stain the colorless separated proteins into distinct brownish-black bands. Silver staining is one of the most sensitive and scalable techniques for visualizing proteins after gel electrophoresis and it is amongst the best colorimetric methods, its performance rival current fluorescent commercial dyes. The conventional methods to visualize the silver-bound proteins require the reduction of the silver ions into metallic grains using a developing solution, making the protein bands brown to black. However, this is a time-dependent reaction which can result in high variability. The rate of development is also uncontrollable, stopping the reduction depends on the operator's determination of the endpoint which is subject to bias leading to further variability. The use of additional chemicals such as sodium thiosulphate and glutaraldehyde acts as a sensitizer to improve the contrast due to the inherently high yellow background staining of silver whilst the latter cross-links proteins to improve the detection limit. Numerous protocols have claimed to excel in one aspect but lack in another, this has motivated us to develop a new silver stain that alleviates the disadvantages associated with the conventional chromogenic methods.

We optimized the silver ion sensitive AIE dye TPE-4TA, a tetraphenylethene (TPE) core tagged with tetrazole rings on each of the four phenyl arms of TPE for our fluorescent silver (silver-AIE) protein gel staining protocol. Our probe is estimated to have a limit of detection of 2.3 nM or 0.25 μgL^{-1} for silver ions (99). The protocol developed as described in this paper requires one thousand-fold less silver nitrate concentration needed for staining protein gels compared to 0.1% found in commonly used silver nitrate protocols. Using an unstained protein ladder with consecutive two-fold dilutions in NuPAGE™ 4-12% Bis-Tris protein gels (1.0 mm thick gels). We compared our new silver-AIE method with traditional silver nitrate and the commercial SYPRO ruby fluorescent stain in terms of sensitivity (detection performance), linearity (quantitative performance) and differential

protein detection. Our protocol was able to show that traditional silver staining had the lowest limit of detection (LLD) of 1-10 ng band^{-1}, whereas our method showed 1-16-fold lower LLD (more sensitive). When compared to the SYPRO Ruby stain, our sensitivity was greater by 1-8-fold. The silver-AIE method also shows good quantitative performance, we compared the linear dynamic range (LDR) and found that it had a linearity (R^2 = 0.960) greater than its traditional silver counterpart (R^2 = 0.819) yet comparable to SYPRO Ruby (R^2 = 0.957) (99). This is important as traditional silver developing methods which sometimes exhibit non-uniform staining are not recommended for quantification.

4.2 Paper II: A Modernised Fluorescent Silver Method For 3D Brain Histology Using an AIE Fluorogenic Probe.

Small molecule organic fluorescent dyes for visualizing 3D cleared tissue are becoming more in demand (91) as clearing methods that do not require additional instruments are highly accessible to researchers. 3D imaging of the human brain can help us to understand how the brain functions, this would require large-scale mapping of the brain under a variety of diseases.

The development of the passive CLARITY technique (100,101) has allowed for large specimens such as the intact mouse brain to be transparent for imaging with advanced microscopes. Staining with immunofluorescence would not be practical at high throughput, especially with large samples. It may also be highly variable with human tissue as cold ischemia time, agonal state and post-mortem time vary for each sample. Furthermore, fluorescent proteins or viral tracers would not be appropriate for human specimens, which is why small-molecule fluorescent dyes would be an attractive option. AIE luminogens are easily scalable and can be very photostable, making them suitable to withstand long and repeated imaging sessions.

Using an AIE-based silver sensor, TPE-4TA We hypothesize that the silver-AIE staining protocol can be adapted to enhance the visualization of neurons and fibers in both paraffin-embedded sections and CLARITY-cleared tissue. This could provide an efficient and powerful tool for brain mapping and pathological studies of neural tissue; it could also facilitate co-staining with immunofluorescence techniques to further enhance the identification and characterization of specific cell populations. Silver is incredibly versatile and can stain different targets of interest in the brain. Many protocols have also reported staining different cells and structures of interest besides neurons, such as nerve fibers, glia, and amyloid plaques. Therefore, the use of silver-AIE staining could have wide-ranging applications in neuroscience research, including the study of neural development, plasticity, and neurodegeneration.

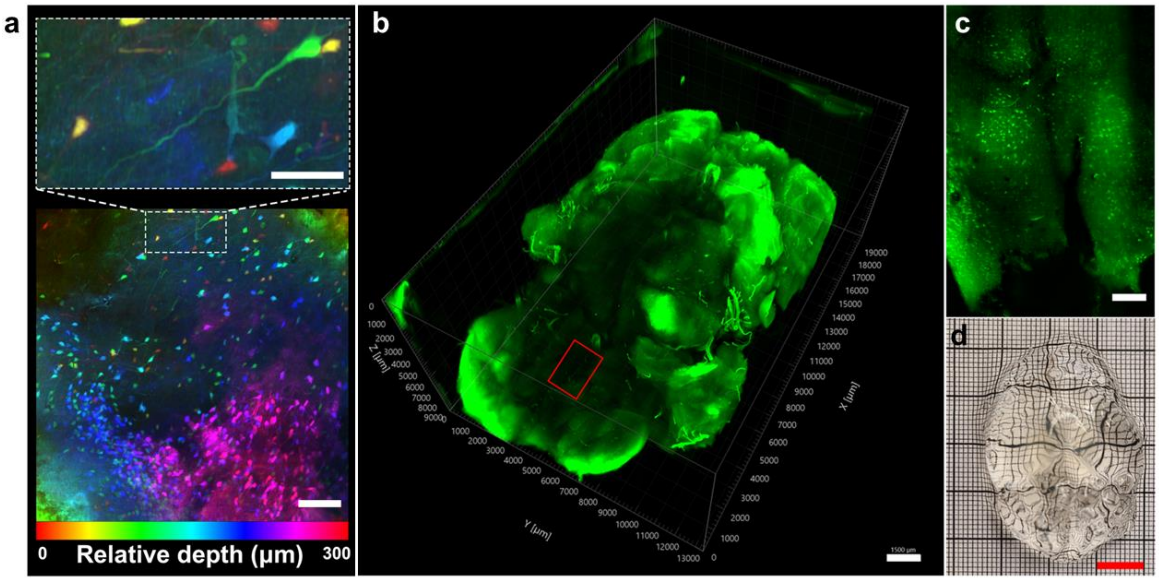

Figure 22. Light sheet imaging of passive CLARITY cleared thick tissue and the whole brain was stained with silver-AIE. a, Depth-coded z-stack projection of a cleared C57BL/6 mouse brain tissue slabs stained with the fluorogenic silver-AIE method, imaged using the Zeiss light sheet 7 microscopes with a depth of 300 µm. Scale bar: 100 µm. Inset shows a zoom-in of a neuron. Scale bar: 30 µm. **b,** cleared the whole brain with silver-AIE imaged on the LiToneXL light-sheet microscope.

Passive CLARITY uses the same monomers to make the polyacrylamide gels used in SDS-PAGE, which is a common reagent in most labs. Our method is accessible to many labs, we successfully imaged cleared mouse brain tissue using standard widefield epifluorescence microscopes in addition to advanced microscopes such as confocal, multiphoton, and light sheet microscopy (Fig. 22). Because of the highly sensitive nature of the fluorogenic AIE probe due to the tetrazole moieties, our results show that the silver-AIE method requires substantially less silver nitrate to stain both neurons and myelinated fibers with a concentration of 0.005% in 8 µm thick paraffin sections and 0.00001% in passively cleared tissue, which is two million-fold lower than the standard modified Bielschowsky silver method (102). It is also a less hazardous and scalable method to visualize the brain than traditional silver protocols. We also found that the cells stained by the silver-AIE method stain approximately 37.4% of NeuN-positive neurons and does not stain astrocytes in paraffin tissue sections (Fig. 23) when labelled for glial fibrillary acidic protein (GFAP), which further supports its selectivity of the staining method to neuronal cells.

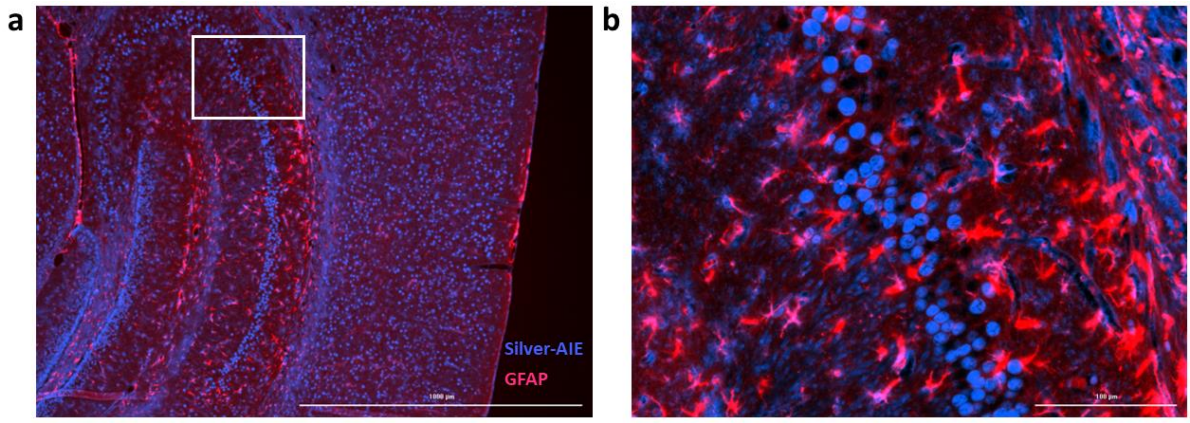

Figure 23. Silver-AIE stained coronal mouse brain co-labelled with glial fibrillary acidic protein (GFAP). a, overview of the cortex and hippocampus from a wild-type mouse immunostained for GFAP (red) with Alexa 647 co-labelled with silver-AIE (blue) scale bar, 1000 µm. **b,** magnified view of the region of interest (white box) from **a**. scale bar 100 µm.

4.3 Paper III: A Near-Infrared AIE Fluorescent Probe for Myelin Imaging: from Sciatic Nerve to the Optically Cleared Brain Tissue in 3D.

Fluorescent probes can allow the visualization of myelinated fibers, fascicles, and long projecting fiber tracts in 3D, which can help researchers to understand the pathology of 3D demyelinating diseases. Chemical probes for myelin in cleared tissue are not often reported and existing myelin-specific probes have poor tissue permeability or suffer from low-signal-to-background ratio. Assessing the fiber distribution and size of the white matter (wm) tracts in animal models allows for evaluating the effectiveness of treatments.

We developed a near-infrared (NIR) AIE probe called PM-ML compatible with clearing methods for 3D deep tissue imaging. It has selectivity to myelin with good contrast and photostability for imaging-cleared mouse brain tissue and the fixed sciatic nerve. PM-ML has a non-planar conformation which is responsible for its AIE attributes. The D–π–A structure of PM-ML affords the NIR wavelength emission, and it has a maximum absorption peak of 495 nm in DMSO and emission at 708 nm in a solid state with a stoke shift of 213 nm. The binding capacity of PM-ML to phospholipids were evaluated with photoluminescence spectrometry using the common models 2-dioleoyl-sn-glycero-3-phosphocholine (DOPC) and 2-oleoyl-1-palmitoyl-snglycero-3-phosphocholine (POPC) in PBS. A significant fluorescent intensity enhancement can be observed, suggesting incorporation of the PM-ML dye into the phospholipid bilayer causing restriction of intramolecular motion of PM-ML.

PM-ML is very biocompatible and allows the selective staining of the plasma membrane in live cells in addition to fixed mammalian cells as demonstrated in RAW264.7, NIH 3T3 and HeLa cells. We first demonstrated PM-ML 3D labelling capabilities of myelin in fixed tissue sections from young C57BL/6J mice (P18) cleared with Clear^{T}. In the 3D reconstruction, PM-ML showed distinct fibers at high magnification in the caudate

putamen (CPu) with good contrast compared to FluoroMyelin Green/Red which had a high background. Furthermore, in the cleared tissue samples, FluoroMyelin Green/Red completely faded out when imaged after storage in 4 ˚C for 3 weeks. In contrast, PM-ML could allow imaging of myelin even after 5 months of storage. PM-ML can also visualize the node of Ranvier and Schmidt-Lanterman incisures in the fixed sciatic nerve.

The *Shiverer* mutation in the mouse model is a deletion mutation in the myelin basic protein (MBP) gene that causes the loss of the myelin sheath in the CNS. Selectivity of PM-ML to myelin was demonstrated by staining cleared *Shiverer* brain sections which had no signal when stained with PM-ML compared to the heterozygous *Shiverer* Mbp^{shi}/Mbp^{+} and C57BL/6J WT control mice. PM-ML displayed a high signal-to-background ratio compared with other commercial probes FluoroMyelin Green/Red and Vybrant DiD. The addition of Triton X- 100 detergent is necessary for Vybrant DiD staining of myelin; however, this can potentially damage fine structures by extracting lipid. Such permeabilization treatment is not needed for PM-ML staining. The performance of PM-ML makes it a suitable probe for studying and imaging myelinated fibers with a high-penetration depth in 3D-cleared tissue.

5 Conclusions

Tissue clearing and optical sectioning microscopy combined with fluorescent staining methods will enable high-resolution mapping and 3D visualization of fine structures. Demand for fluorescent labelling methods with ease of use, high photostability, reliability and scalability are of great interest, especially when it comes to human samples. Many Conventional fluorophores display ACQ characteristics which limit the application of the dye at high concentrations. In 2001, an opposite phenomenon to ACQ known as AIE was discovered. This spurred the development of numerous AIE luminogens with "turn-on" properties that showed high brightness and photostability in the solid state. This means a bright fluorescence can be retained when aggregated without quenching or when applied at a very high concentration, making AIE luminogens an attractive choice for the labelling of 3D-cleared tissue.

The development of novel fluorescent tools and techniques for 3D imaging of cleared brains is crucial for making important advances in the field of neuroscience. One of the major challenges in the field is the need for new tissue labelling technologies. Existing methods such as immunostaining have limitations and drawbacks, including the need for optimal fixation and requires a large amount to stain tissue. This has spurred interest in developing alternative strategies for visualizing the optically transparent brain, especially from fixed archived samples or human autopsies that are not optimally fixed. AIE-based probes and methods provide a reliable and robust alternative to traditional tissue labelling techniques.

In conclusion, this thesis aimed to develop alternative strategies for 3D neural tissue labelling using novel AIE turn-on probes in the mouse brain with various microscopes.

1) To develop a new fluorogenic silver technique for bio-staining called silver-AIE, this protocol by utilised a water-soluble silver ion-sensitive AIE probe TPE-4TA for the silver-AIE staining of proteins in SDS-PAGE gels, we demonstrated that fluorogenic development could ameliorate the drawbacks of traditional colorimetric silver methods. The new method shows little to no background staining in the polyacrylamide gels with a superior linear relationship for quantification.

2) The silver-AIE technique was then further optimised and adapted into neurons and nerve fibres in paraffin sections and passive CLARITY cleared mouse brain tissue for 3D fluorescent imaging. We investigated the silver-AIE specificity to neurons and its staining performances in different regions of the brain. Approximately 34.7% of NeuN-positive neurons are colocalized with silver-AIE, this is much greater than 1-3% reported in the Golgi stain. However, Purkinje and olfactory mitral cells do not express Rbfox3/NeuN which can instead be visualized by silver-AIE.

This fluorogenic method may serve as a 3D counterstain for neurons, it uses less hazardous chemicals, and the extremely low concentration may allow for other downstream analyses.

3) The AIEgen PM-ML with D–π–A structure is a plasma membrane targeting dye that is also specific to myelin. We demonstrated myelin staining with PM-ML in cryosections using confocal microscopy and 3D imaging with both confocal and two-photon microscopy of Clear^{T} cleared tissue sections. The Schmidt-Lanternman incisures and node of Ranvier can also be detected in the fixed sciatic nerve. The performance of PM-ML as a probe for studying and imaging myelinated fibers in 3D-cleared tissue is of major interest with the potential to greatly aid in the study of demyelinating diseases such as multiple sclerosis.

6 Points of perspective

As tissue clearing and microscopes continue to develop for larger specimens, the demand for a robust and practical labelling method will be greater. Researchers have demonstrated clearing and imaging of the intact whole mouse body using vDISCO and light-sheet microscopy. At this scale, changes to the labelling method to accommodate such as sample have been made, such as the application of nanobody conjugation to bright far-red dyes for better tissue penetration whilst also mitigating the shorter wave autofluorescence (103).

To better study the human brain, efforts in progressing 3D histology techniques are needed to facilitate discoveries and evaluate treatments and therapies. Adult human organs are especially challenging to optically clear due to the highly dense molecules that have accumulated throughout the decades. It is now possible to clear the entire intact human brain with the SHANEL method thanks to new detergent permeabilization chemistry and organic solvents (51). To image such a large specimen, the demand for a practical labelling method is highly desired. Chemical fluorescent labelling techniques with near-infrared emission have enormous potential and practicality for deep tissue imaging. Near infrared AIE dyes with short step-synthesis could be a viable option for labelling of archived human tissue given the excellent photostability and scalability. A silver sensitive probe with far red emission would be a good tool for mapping or revisiting archived samples, especially if the probe is not pH dependent.

The limitations in fluorescence microscopy not only includes the chemistry of the fluorophore but also microscope optics and the laser exposure of the sample. Obtaining good spatial resolution requires trade-offs with image acquisition speed and light exposure. Computational methods can be employed to facilitate faster imaging speeds whilst minimizing these trade-offs. This could be achieved by content aware image restoration with deep learning (104). Once a model is trained with ground truth data, images be acquired quickly with lower laser power to reduce photobleaching and a lower averaging is needed which can lead to faster imaging.

Given the interests to image the 3D whole mouse brain at single cell resolution, there will be similar challenges with generating 3D maps of human organs. The Incredibly large datasets generated will require new solutions for practical imaging acquisition times, data storage and analysis. Cloud based computing may offer a practical solution for storage these large datasets whilst convenient for accessibility and viewing of data, especially when a high-performance computer is not available. An example is the CUBIC-Cloud framework which allows registration, sharing and publication of whole mouse-brain datasets (105).

7 Acknowledgements

I would like to sincerely thank my supervisor **Dr. Sijie Chen.** I am grateful that you allow me to be your PhD student, thank you for your supervision and the opportunity to work in your lab at the Ming Wai Lau Centre for reparative medicine (MWLC). Without your ideas, support and remarks the projects could not have been conducted. It has been great working with you and watching your lab grow throughout the years.

To my co-supervisors: **Prof. Ola Hermanson**, I am grateful for your guidance, support, and advice. I really enjoyed my time in your lab. I've also become a fan of the Big Wave Bay song (and the drink)! Thank you **Prof. Per Uhlén** for the discussions and inspiration.

I also appreciate the support and lessons from **Sylvie Le Guyader** (thank you for also being chairperson) and **Gabriela Imreh** at the LCI facility. I really enjoyed the microscopy course!

It is with immense gratitude that I acknowledge the support and help of **Dr. Sheng Xie** and **Dr. Ming-Yu Wu,** without your dyes I could not have completed my work. I do appreciate all the support, help and kind suggestions given to me by my current and former lab members. **Kam Chuen, Quanzhi Yang**, **Deshuang Tu, Fei Wang, Miller Leung, Renee Chou, Hui Gao, Blake Ho, Steven Zhao,** and **Chloe Lee**.

Thank you to everyone at MWLC for your support throughout my time at the centre.

Sandra, Agneta and **Anna Däckfors,** I am incredibly grateful to you for supporting me in HK and in Stockholm. Thanks for making sure my PhD journey was practical. You were very welcoming, kind and caring during my time in HK and at biomedicum.

Special thanks to the former and current members of the admin and technical team **Emily**, **Patrick, Molly, Charlie, Heather, Anna Chan, Venus,** and **Eva**. You have kept the centre and lab running smoothly even through tough times so we can still progress with our work. I really appreciate it. **Virpi** and **Callum**, I really appreciate your feedback and support in helping me improve my presentation skills. Thank you **Bangheng (Conrad)** for sharing some reagents/consumables (including the snack kind!) during my studies.

I am sincerely grateful for the help and support I received from collaborators at The University of Hong Kong. **Gale**, I am extremely happy to be your friend your intellect and passion for science never ceases to amaze me. Hope we can continue to be collaborators in the future. Thank you, **Kenneth**, for teaching me how to extract the mouse brain, cryosectioning, providing Shiverer mouse models/samples and discussion on the projects. I wish you all the best in the UK. **Sharon**, I am sincerely thankful for your patch clamp experiments, I have learnt so much from you, and appreciate your support and kindness. Thank you, **Prof. Y.S Chan** for the support at The University of Hong Kong and others in the lab for ensuring a smooth collaboration.

Many thanks to the collaborators at Hong Kong University of Science and Technology, thank you **Prof. Nancy Ip** and **Prof. Kai Liu** for the support and providing samples. I also appreciate the support from the engineers at Light innovation technology for helping me image my sample with the LiToneXL instrument when I was on courses outside of HK and during COVID isolation.

I would also like to thank **Dennis Tsim** and **Priscilla Ngai** from Chinetek Scientific for their assistance and access to Nikon microscopes.

My fiancée and mentor **Bonnie**, thank you so much for your support, proofing my thesis and waiting in HK. I am truly grateful. You have been very inspirational and motivating. I could not have gotten this far without you, keeping me upright and moving forward. I can't wait to start a new journey with you.

Christina, Alkis, and **Samuel**, I am glad to have met you guys in Toronto and work with you in Stockholm, thanks for looking out for me. **Mykola**, I am impressed with your paintballing skills! Thanks for the hand warmers too. I would also like to extend my thanks to others at 7D for your support. My student experience at KI would not be complete without your kindness.

Fred and **Sarah,** some unforgettable memories were made in Toronto! The conference you organized is one of the best I've been to so far!

I would also like to thank my family and my brother **Harvey** for their endless support.

8 References

1. Jing D, Zhang S, Luo W, Gao X, Men Y, Ma C, et al. Tissue clearing of both hard and soft tissue organs with the pegasos method. Cell Res. 2018;28(8):803–18.

2. Engelborghs Y, Visser AJWG, editors. Fluorescence Spectroscopy and Microscopy. Totowa, NJ: Humana Press; 2014. (Methods in Molecular Biology; vol. 1076).

3. Lichtman JW, Conchello JA. Fluorescence microscopy. Nat Methods. 2005;2(12):910–9.

4. Jerome WGJ, Price RL. Basic Confocal Microscopy. 2nd ed. Springer Cham; 2018. p. 21–36.

5. Suzuki S, Sasaki S, Sairi AS, Iwai R, Tang BZ, Konishi G. Principles of Aggregation-Induced Emission: Design of Deactivation Pathways for Advanced AIEgens and Applications. Angew Chem., Int Ed. Engl. 2020;132(25):9940–51.

6. Lakowicz JR. Fluorophores - Principles of Fluorescence Spectroscopy. 3rd ed. New York, NY: Springer; 2006. p. 63–95. Available from: https://doi.org/10.1007/978-0-387-46312-4_3

7. Huang Y, Zhang Y, Huo F, Wen Y, Yin C. Design strategy and bioimaging of small organic molecule multicolor fluorescent probes. Sci China Chem. 2020 Dec 21;63(12):1742–55.

8. Terai T, Nagano T. Small-molecule fluorophores and fluorescent probes for bioimaging. Vol. 465, Pflug Arch Eur J Phy. 2013. p. 347–59.

9. Zimmer M. Green Fluorescent Protein (GFP): Applications, Structure, and Related Photophysical Behavior. Chem Rev. 2002 Mar 1;102(3):759–82.

10. Day RN, Davidson MW. The fluorescent protein palette: tools for cellular imaging. Chem Soc Rev. 2009;38(10):2887.

11. Tsien RY. Constructing and Exploiting the Fluorescent Protein Paintbox (Nobel Lecture). Angew Chem., Int Ed Engl. 2009 Jul 20;48(31):5612–26.

12. Sample V, Newman RH, Zhang J. The structure and function of fluorescent proteins. Chem Soc Rev [Internet]. 2009;38(10):2852. Available from: http://xlink.rsc.org/?DOI=b913033k

13. Dobbie IM, Lowndes NF, Sullivan KF. Autofluorescent Proteins. In 2008. p. 1–22. Available from: https://linkinghub.elsevier.com/retrieve/pii/S0091679X08850017

14. Frommer WB, Davidson MW, Campbell RE. Genetically encoded biosensors based on engineered fluorescent proteins. Chem Soc Rev. 2009;38(10):2833.

15. Rodriguez EA, Campbell RE, Lin JY, Lin MZ, Miyawaki A, Palmer AE, et al. The Growing and Glowing Toolbox of Fluorescent and Photoactive Proteins. Trends Biochem Sci [Internet]. 2017 Feb;42(2):111–29. Available from: https://linkinghub.elsevier.com/retrieve/pii/S0968000416301736

16. Han X, Xu K, Taratula O, Farsad K. Applications of nanoparticles in biomedical imaging. Nanoscale. 2019;11(3):799–819.

17. Miu BA, Dinischiotu A. New Green Approaches in Nanoparticles Synthesis: An Overview. Molecules. 2022 Oct 1;27(19):6472.

18. Bonilla CAM, Kouznetsov V v. "Green" Quantum Dots: Basics, Green Synthesis, and Nanotechnological Applications. In: Green Nanotechnology - Overview and Further Prospects. InTech; 2016.

19. Singh J, Dutta T, Kim KH, Rawat M, Samddar P, Kumar P. 'Green' synthesis of metals and their oxide nanoparticles: applications for environmental remediation. J Nanobiotechnology. 2018 Dec 30;16(1):84.

20. Hong Y, Lam JWY, Tang BZ. Aggregation-induced emission. Chem Soc Rev. 2011;40(11):5361.

21. Wang H, Zhao E, Lam JWY, Tang BZ. AIE luminogens: emission brightened by aggregation. Materials Today. 2015 Sep;18(7):365–77.

22. Mei J, Leung NLC, Kwok RTK, Lam JWY, Tang BZ. Aggregation-Induced Emission: Together We Shine, United We Soar! Chem Rev [Internet]. 2015 Nov 11;115(21):11718–940. Available from: https://pubs.acs.org/doi/10.1021/acs.chemrev.5b00263

23. Hong Y, Lam JWY, Tang BZ. Aggregation-induced emission. Chem Soc Rev. 2011;40(11):5361.

24. Luo J, Xie Z, Lam JWY, Cheng L, Tang BZ, Chen H, et al. Aggregation-induced emission of 1-methyl-1,2,3,4,5-pentaphenylsilole. Chem Comm. 2001;(18):1740–1.

25. Leung NLC, Xie N, Yuan W, Liu Y, Wu Q, Peng Q, et al. Restriction of intramolecular motions: The general mechanism behind aggregation-induced emission. Chem Eur J. 2014;20(47):15349–53.

26. He Z, Tian S, Gao Y, Meng F, Luo L. Luminescent AIE Dots for Anticancer Photodynamic Therapy. Vol. 9, Front Chem. Frontiers Media S.A.; 2021.

27. Gutiérrez-Arzaluz L, Nadinov I, Healing G, Czaban-Jóźwiak J, Jia J, Huang Z, et al. Ultrafast Aggregation-Induced Tunable Emission Enhancement in a Benzothiadiazole-Based Fluorescent Metal–Organic Framework Linker. J Phys Chem B. 2021 Dec 9;125(48):13298–308.

28. Wang D, Lee MMS, Xu W, Kwok RTK, Lam JWY, Tang BZ. Theranostics based on AIEgens. Theranostics. 2018;8(18):4925–56.

29. Feng G, Liu B. Aggregation-Induced Emission (AIE) Dots: Emerging Theranostic Nanolights. Acc Chem Res. 2018 Jun 19;51(6):1404–14.

30. Li K, Qin W, Ding D, Tomczak N, Geng J, Liu R, et al. Photostable fluorescent organic dots with aggregation-induced emission (AIE dots) for noninvasive long-term cell tracing. Sci Rep. 2013 Dec 28;3(1):1150.

31. Qin W, Ding D, Liu J, Yuan WZ, Hu Y, Liu B, et al. Biocompatible nanoparticles with aggregation-induced emission characteristics as far-red/near-infrared fluorescent bioprobes for in vitro and in vivo imaging applications. Adv Funct Mater. 2012 Feb 22;22(4):771–9.

32. Hu X, Zhao X, He B, Zhao Z, Zheng Z, Zhang P, et al. A Simple Approach to Bioconjugation at Diverse Levels: Metal-Free Click Reactions of Activated Alkynes with Native Groups of Biotargets without Prefunctionalization. Research. 2018 Dec 12;2018:1–12.

33. Elliott AD. Confocal Microscopy: Principles and Modern Practices. Curr Protoc Cytom. 2020 Mar 26;92(1).

34. Wu Y, Shroff H. Multiscale fluorescence imaging of living samples. Histochem Cell Biol. 2022 Oct 29;158(4):301–23.

35. Oreopoulos J, Berman R, Browne M. Spinning-disk confocal microscopy. In 2014. p. 153–75.

36. Denk W, Strickler JH, Webb WW. Two-Photon Laser Scanning Fluorescence Microscopy. Science (1979). 1990 Apr 6;248(4951):73–6.

37. Benninger RKP, Piston DW. Two-Photon Excitation Microscopy for the Study of Living Cells and Tissues. Curr Protoc Cell Biol. 2013 Jun;59(1).

38. Piston DW. When Two Is Better Than One: Elements of Intravital Microscopy. PLoS Biol. 2005 Jun 14;3(6):e207.

39. Elisa Z, Toon B, de Smedt SC, Katrien R, Kristiaan N, Kevin B. Technical implementations of light sheet microscopy. Microsc Res Tech. 2018 Sep 11;81(9):941–58.

40. Marcos-Vidal A, Ripoll J. Recent advances in optical tomography in low scattering media. Opt Lasers Eng. 2020 Dec;135:106191.

41. Glaser AK, Chen Y, Yin C, Wei L, Barner LA, Reder NP, et al. Multidirectional digital scanned light-sheet microscopy enables uniform fluorescence excitation and contrast-enhanced imaging. Sci Rep. 2018 Sep 17;8(1):13878.

42. Zheng T, Feng Z, Wang X, Jiang T, Jin R, Zhao P, et al. Review of micro-optical sectioning tomography (MOST): technology and applications for whole-brain optical imaging [Invited]. Biomed Opt Express. 2019 Aug 1;10(8):4075.

43. Tian T, Yang Z, Li X. Tissue clearing technique: Recent progress and biomedical applications. Vol. 238, J Anat. Blackwell Publishing Ltd; 2021. p. 489–507.

44. Korytowski W, Sarna T. Bleaching of melanin pigments. Role of copper ions and hydrogen peroxide in autooxidation and photooxidation of synthetic dopa-melanin. J Biol Chem. 1990 Jul;265(21):12410–6.

45. Ueda HR, Ertürk A, Chung K, Gradinaru V, Chédotal A, Tomancak P, et al. Tissue clearing and its applications in neuroscience. Nat Rev Neurosci. 2020 Feb 15;21(2):61–79.

46. Lundvall H. Veiteres iiber Demonstration embryonaler Skelette. von Bardeleben K, Fischer G, editors. 1905.

47. Spalteholz W. A Method for the Clearing of Human and Animal Specimens. S. Hirzel. 1911.

48. Spalteholz W. Über das Durchsichtigmachen von menschlichen und tierischen Präparaten und seine theoretischen Bedingungen, nebst Anhang: Über Knochenfärbung. S. Hirzel. 1914.

49. Dent JA, Polson AG, Klymkowsky MW. A whole-mount immunocytochemical analysis of the expression of the intermediate filament protein vimentin in Xenopus. Development. 1989 Jan 1;105(1):61–74.

50. Erturk A, Becker K, Jahrling N, Mauch CP, Hojer CD, Egen JG, et al. Three-dimensional imaging of solvent-cleared organs using 3DISCO. Nat Protoc. [Internet]. 2012;7(11):1983–95. Available from: https://www.ncbi.nlm.nih.gov/pubmed/23060243

51. Zhao S, Todorov MI, Cai R, -Maskari RA, Steinke H, Kemter E, et al. Cellular and Molecular Probing of Intact Human Organs. Cell. 2020;180(4):796-812.e19.

52. Hama H, Kurokawa H, Kawano H, Ando R, Shimogori T, Noda H, et al. Scale: a chemical approach for fluorescence imaging and reconstruction of transparent mouse brain. Nat Neurosci. 2011 Nov 30;14(11):1481–8.

53. Susaki EA, Tainaka K, Perrin D, Yukinaga H, Kuno A, Ueda HR. Advanced CUBIC protocols for whole-brain and whole-body clearing and imaging. Nat Protoc. 2015 Nov 8;10(11):1709–27.

54. Chung K, Wallace J, Kim SY, Kalyanasundaram S, Andalman AS, Davidson TJ, et al. Structural and molecular interrogation of intact biological systems. Nature [Internet]. 2013 May 16;497(7449):332–7. Available from: http://www.nature.com/articles/nature12107

55. Yang B, Treweek JB, Kulkarni RP, Deverman BE, Chen CK, Lubeck E, et al. Single-Cell Phenotyping within Transparent Intact Tissue through Whole-Body Clearing. Cell. 2014 Aug;158(4):945–58.

56. Murray E, Cho JH, Goodwin D, Ku T, Swaney J, Kim SY, et al. Simple, Scalable Proteomic Imaging for High-Dimensional Profiling of Intact Systems. Cell [Internet]. 2015;163(6):1500–14. Available from: https://www.ncbi.nlm.nih.gov/pubmed/26638076

57. Molbay M, Kolabas ZI, Todorov MI, Ohn T, Ertürk A. A guidebook for DISCO tissue clearing. Mol Syst Biol. 2021 Mar 26;17(3).

58. Merril CR. Development and mechanisms of silver stains for electrophoresis. Acta Histochem Cytochem. 1986;19(5):655–67.

59. Golgi C. Sulla struttura della sostanza grigia del cervello. Gazetta Med Ital. 1873;33:244–6.

60. Bentivoglio M, Cotrufo T, Ferrari S, Tesoriero C, Mariotto S, Bertini G, et al. The original histological slides of Camillo Golgi and his discoveries on neuronal structure. Front Neuroanat. 2019 Feb 18;13.

61. Merchan MA de Castro F. DJ. Cajal and de Castro's Neurohistological Methods. Oxford University Press; 2016.

62. Grant G. Gustaf Retzius (1842–1919). J Neurol. 2011 Apr 5;258(4):706–7.

63. Grizzle WE. Theory and Practice of Silver Staining in Histopathology. J Histotechnol. 1996 Sep 18;19(3):183–95.

64. Peters A. Experiments on the mechanism of silver staining. III. Electron microscope studies. Q. J. Microsc. Sci. 1955;96(March):317–22.

65. Gordon O, Vig Slenters T, Brunetto PS, Villaruz AE, Sturdevant DE, Otto M, et al. Silver Coordination Polymers for Prevention of Implant Infection: Thiol Interaction, Impact on Respiratory Chain Enzymes, and Hydroxyl Radical Induction. Antimicrob Agents Chemother. 2010 Oct;54(10):4208–18.

66. Tao DD, Wang Q, Yan XS, Chen N, Li Z, Jiang YB. Ag + coordination polymers of a chiral thiol ligand bearing an AIE fluorophore. Chem comm [Internet]. 2017;53(1):255–8. Available from: http://xlink.rsc.org/?DOI=C6CC08596B

67. Chuba PJ, Palchaudhuri S. Requirement for cysteine in the color silver staining of proteins in polyacrylamide gels. Anal Biochem. 1986 Jul;156(1):136–9.

68. Grimelius L. Silver stains demonstrating neuroendocrine cells. Biotech. Histochem. 2004 Feb 12;79(1):37–44.

69. Westermark P. Lars Grimelius and his silver impregnation method—Commentaries on the paper in *Upsala Journal of Medical Sciences* with the highest number of citations. Ups J Med Sci. 2015 Mar 17;1–4.

70. Parkinson M, Mortimer A. Bancroft's Theory and Practice of Histological Techniques. 2013. p. 73–249

71. Litchfield S, Nagy Z. New temperature modification makes the Bielschowsky silver stain reproducible. Acta Neuropathol. 2001 Jan;101(1):17–21.

72. Spacek J av. Dynamics of golgi impregnation in neurons. Microsc Res Tech. 1992 Dec 1;23(4):264–74.

73. Zaqout S, Kaindl AM. Golgi-Cox Staining Step by Step. Front Neuroanat. 2016 Mar 31;10.

74. Vints K, Vandael D, Baatsen P, Pavie B, Vernaillen F, Corthout N, et al. Modernization of Golgi staining techniques for high-resolution, 3-dimensional imaging of individual neurons. Sci Rep [Internet]. 2019;9(1):130. Available from: https://www.ncbi.nlm.nih.gov/pubmed/30644431

75. Ovchinnikov O, Aslanov S, Smirnov M, Perepelitsa A, Kondratenko T, Selyukov A, et al. Colloidal Ag_2 S/SiO_2 core/shell quantum dots with IR luminescence. Opt Mater Express. 2021 Jan 1;11(1):89.

76. Tang R, Xue J, Xu B, Shen D, Sudlow GP, Achilefu S. Tunable Ultrasmall Visible-to-Extended Near-Infrared Emitting Silver Sulfide Quantum Dots for Integrin-Targeted Cancer Imaging. ACS Nano. 2015 Jan 27;9(1):220–30.

77. Yan D, He Y, Ge Y, Song G. Fluorescence "turn on-off" detection of heparin and heparinase I based on the near-infrared emission polyethyleneimine capped Ag2S quantum dots. Sens Actuators B Chem. 2017 Mar;240:863–9.

78. Thompson KJ, Harley CM, Barthel GM, Sanders MA, Mesce KA. Plasmon resonance and the imaging of metal-impregnated neurons with the laser scanning confocal microscope. Elife [Internet]. 2015 Dec 15;4. Available from: https://elifesciences.org/articles/09388

79. Yan N, Tang BZ, Wang WX. In Vivo Bioimaging of Silver Nanoparticle Dissolution in the Gut Environment of Zooplankton. ACS Nano. 2018;12(12):12212–23.

80. Bilberg K, Hovgaard MB, Besenbacher F, Baatrup E. In Vivo Toxicity of Silver Nanoparticles and Silver Ions in Zebrafish (Danio *rerio*). J Toxicol. 2012;2012:1–9.

81. Singha S, Kim D, Seo H, Cho SW, Ahn KH. Fluorescence sensing systems for gold and silver species. Chem Soc Rev. 2015;44(13):4367–99.

82. Shi W, Sun S, Li X, Ma H. Imaging Different Interactions of Mercury and Silver with Live Cells by a Designed Fluorescence Probe Rhodamine B Selenolactone. Inorg Chem. 2010 Feb 1;49(3):1206–10.

83. Liu L, Zhang G, Xiang J, Zhang D, Zhu D. Fluorescence "Turn On" Chemosensors for Ag + and Hg 2+ Based on Tetraphenylethylene Motif Featuring Adenine and Thymine Moieties. Org Lett [Internet]. 2008 Oct 16;10(20):4581–4. Available from: https://pubs.acs.org/doi/10.1021/ol801855s

84. Herculano-Houzel S. The remarkable, yet not extraordinary, human brain as a scaled-up primate brain and its associated cost. Proc. Natl. Acad. Sci. U.S.A. 2012 Jun 26;109(supplement_1):10661–8.

85. Chen TW, Wardill TJ, Sun Y, Pulver SR, Renninger SL, Baohan A, et al. Ultrasensitive fluorescent proteins for imaging neuronal activity. Nature. 2013 Jul 18;499(7458):295–300.

86. Dunn M, Boltaev U, Beskow A, Pampou S, Realubit R, Meira T, et al. Identification of Fluorescent Small Molecule Compounds for Synaptic Labeling by Image-Based, High-Content Screening. ACS Chem Neurosci. 2018 Apr 18;9(4):673–83.

87. Wessendorf MW. Fluro-Gold: composition, and mechanism of uptake. Brain Res [Internet]. 1991 Jul;553(1):135–48. Available from: https://linkinghub.elsevier.com/retrieve/pii/000689939190241M

88. Alvarez-Buylla A, Ling CY, Kirn JR. Cresyl violet: A red fluorescent Nissl stain. J Neurosci Methods. 1990 Aug;33(2–3):129–33.

89. Rajasekhar K, Narayanaswamy N, Murugan NA, Kuang G, Ågren H, Govindaraju T. A High Affinity Red Fluorescence and Colorimetric Probe for Amyloid β Aggregates. Sci Rep. 2016 Apr 1;6(1):23668.

90. Schmued LC, Albertson C, Slikker W. Fluoro-Jade: a novel fluorochrome for the sensitive and reliable histochemical localization of neuronal degeneration. Brain Res. 1997 Mar;751(1):37–46.

91. Lai HM, Ng WL, Gentleman SM, Wu W. Chemical Probes for Visualizing Intact Animal and Human Brain Tissue. Cell Chem Biol [Internet]. 2017;24(6):659–72. Available from: http://dx.doi.org/10.1016/j.chembiol.2017.05.015

92. Monsma PC, Brown A. FluoroMyelin™ Red is a bright, photostable and non-toxic fluorescent stain for live imaging of myelin. J Neurosci Methods [Internet]. 2012 Aug;209(2):344–50. Available from: https://linkinghub.elsevier.com/retrieve/pii/S0165027012002403

93. Zhu X, Huang L, Zheng Y, Song Y, Xu Q, Wang J, et al. Ultrafast optical clearing method for three-dimensional imaging with cellular resolution. Proc. Natl. Acad. Sci. U.S.A. [Internet]. 2019 Jun 4;116(23):11480–9. Available from: http://www.pnas.org/lookup/doi/10.1073/pnas.1819583116

94. Hill RA, Grutzendler J. Uncovering the biology of myelin with optical imaging of the live brain. Glia. 2019 Nov 29;67(11):2008–19.

95. Hill RA, Grutzendler J. Uncovering the biology of myelin with optical imaging of the live brain. Glia [Internet]. 2019 Nov 29;67(11):2008–19. Available from: https://onlinelibrary.wiley.com/doi/10.1002/glia.23635

96. Jin LT, Hwang SY, Yoo GS, Choi JK. Sensitive silver staining of protein in sodium dodecyl sulfate-polyacrylamide gels using an azo dye, calconcarboxylic acid, as a silver-ion sensitizer. Electrophoresis [Internet]. 2004 Aug;25(15):2494–500. Available from: http://doi.wiley.com/10.1002/elps.200306002

97. Peters.A. A general-purpose method of silver staining. Scientific and Industrial journal. 1955;96(1948):323–8.

98. Yun SW, Kang NY, Park SJ, Ha HH, Kim YK, Lee JS, et al. Diversity Oriented Fluorescence Library Approach (DOFLA) for Live Cell Imaging Probe Development. Acc Chem Res. 2014 Apr 15;47(4):1277–86.

99. Xie S, Wong AYH, Kwok RTK, Li Y, Su H, Lam JWY, et al. Fluorogenic Ag+–tetrazolate aggregation enables efficient fluorescent biological silver staining. Angewandte Chemie - International Edition. 2018;57(20):5750–3.

100. Neckel PH, Mattheus U, Hirt B, Just L, Mack AF. Large-scale tissue clearing (PACT): Technical evaluation and new perspectives in immunofluorescence, histology and ultrastructure. Sci Rep. 2016 Sep 29;6(1):34331.

101. Phillips J, Laude A, Lightowlers R, Morris CM, Turnbull DM, Lax NZ. Development of passive CLARITY and immunofluorescent labelling of multiple proteins in human cerebellum: understanding mechanisms of neurodegeneration in mitochondrial disease. Sci Rep [Internet]. 2016 Sep 16;6(1):26013. Available from: http://www.nature.com/articles/srep26013

102. Yamamoto T, Hirano A. A comparative study of modified Bielschowsky, Bodian and Thioflavin S stains on Alzheimer's neurofibrillary tangles. Neuropathol Appl Neurobiol. 1986 Jan;12(1):3–9.

103. Cai R, Pan C, Ghasemigharagoz A, Todorov MI, Förstera B, Zhao S, et al. Panoptic imaging of transparent mice reveals whole-body neuronal projections and skull–meninges connections. Nat Neurosci. 2019 Feb 31;22(2):317–27.

104. Weigert M, Schmidt U, Boothe T, Müller A, Dibrov A, Jain A, et al. Content-aware image restoration: pushing the limits of fluorescence microscopy. Nat Methods. 2018 Dec;15(12):1090–7.

105. Mano T, Murata K, Kon K, Shimizu C, Ono H, Shi S, et al. CUBIC-Cloud provides an integrative computational framework toward community-driven whole-mouse-brain mapping. Cell Rep Methods. 2021 Jun;1(2):100038.